Chemical Geology 690 (2025) 122839

Contents lists available at ScienceDirect

Chemical Geology

journal homepage: www.elsevier.com/locate/chemgeo

Research Paper

Trace elements and iron speciation analysis of Paleoproterozoic phyllite from the Gandarela Syncline: Implications for salinity and redox conditions in the Quadrilátero Ferrífero, Brazil ☆

Janaina Rodrigues de Paula [a], Wei Wei [b,c,*], Fabricio A. Caxito [a], Katherine N. Snihur [c], Cody N. Lazowski [c], Kurt O. Konhauser [c], Erik A. Sperling [d], Daniel S. Alessi [c]

[a] *Universidade Federal de Minas Gerais, Programa de Pós-graduação em Geologia, Instituto de Geociências, Departamento de Geologia, CPMTC-IGC, 31270-901, Brazil*
[b] *School of Earth Science, China University of Geosciences (Wuhan), Wuhan 430074, Hubei Province, China*
[c] *Department of Earth and Atmospheric Sciences, University of Alberta, 1-26 Earth Sciences Building, Edmonton T6G 2E3, Alberta, Canada*
[d] *Department of Geological Sciences, Stanford University, Stanford 94305-2115, CA, USA*

ARTICLE INFO

Editor: Karen Johannesson

Keywords:
Paleosalinity
Redox-sensitive elements
Cauê BIF
Minas Supergroup
Paleoenvironmental reconstruction

ABSTRACT

The Quadrilátero Ferrífero, Brazil, is among the most significant iron ore provinces. This study utilizes geochemical proxies, including elemental paleosalinity ratios (B/Ga, Sr/Ba, S/TOC), redox-sensitive elements (RSE), and iron speciation, to investigate water mass evolution. Samples were analyzed from three drill cores and four outcrops in the Gandarela Syncline, providing new insights into the Paleoproterozoic phyllites associated with the Cauê BIF. Although metamorphism of these rocks might affect the application of the proxy, consistent directional trends in proxy results indicate a refined and/or robust paleoenvironmental reconstruction of the Minas Basin. Paleosalinity data indicate a transition from freshwater to low-brackish conditions during early sedimentation (Caraça Formation), followed by predominantly marine conditions during the deposition of the Cauê, Gandarela, and Cercadinho Formations. This model revises earlier interpretations suggesting an initial dominance of marine facies during fine sediment deposition in the Batatal Formation. Elevated concentrations of trace elements (Cu, Ni, and Zn) in carbonaceous phyllites highlight the role of microbial activity in bioproductivity before BIF deposition. Additionally, the decreasing enrichment factor $_{(EF)}$ of Mo_{EF}/U_{EF} ratio and RSE concentrations toward younger rocks, coupled with variations in Fe_{HR} (highly reactive iron), suggest that the early basin waters were characterized by anoxic to suboxic conditions, with free O_2 likely present in surface waters. These results point to a stratified water column, featuring an oxic surface layer overlying ferruginous, anoxic water. This study advances understanding of the paleoenvironmental evolution of the Minas Basin and the depositional processes that facilitated the formation of the Quadrilátero Ferrífero's giant iron deposits. It also underscores the value of paleosalinity proxies for reconstructing environmental conditions in Paleoproterozoic systems, while also highlighting the need for more studies of how paleoenvironmental proxies behave during metamorphism.

1. Introduction

The Quadrilátero Ferrífero is among Brazil's most important iron ore deposits (Dorr, 1969; Rosière and Chemale Jr, 2000; Hagemann et al., 2016). In addition to the economic benefits, Banded Iron Formations (BIF) are chemical archives of Precambrian seawater and therefore integral for understanding the evolution of early Earth (Spier et al., 2007; Konhauser et al., 2017). Previous research has suggested that the Paleoproterozoic rocks in this region were primarily deposited in a partially oxidized ocean (e.g. Spier et al., 2007; Rosière et al., 2008; Mendes et al., 2017). Several studies have been carried out on trace elements and stable isotopes such as carbon (C), iron (Fe), chromium (Cr), and oxygen (O_2) in BIF and associated carbonate rocks. Studies by Bekker et al. (2003), Morgan et al. (2013), Teixeira et al. (2017), Sampaio et al. (2018), and De Paula et al. (2023) have discussed the role of dissimilatory iron reduction (DIR) in the diagenesis of the primary iron-

---

☆ This article is part of a Special issue entitled: 'Elemental salinity proxies' published in Chemical Geology.

* Corresponding author at: School of Earth Science, China University of Geosciences (Wuhan), Wuhan 430074, Hubei Province, China.
E-mail address: weiwei910911@163.com (W. Wei).

https://doi.org/10.1016/j.chemgeo.2025.122839
Received 28 February 2025; Received in revised form 4 May 2025; Accepted 7 May 2025

rich mineral phases comprising BIF. These studies have also correlated the iron deposits of the Quadrilátero Ferrífero with other Paleoproterozoic giant Fe deposits in South Africa and Western Australia. Despite these advances, no investigations have focused on paleo-salinity and its relationship with redox conditions within the Quadrilátero Ferrífero. This gap underscores the limited understanding of paleo-water mass evolution in this region, obscuring the formation mechanism of the BIF developed in this area. Therefore, an integrated approach is imperative to obtain more insight into the depositional reconstruction of this geological region and improve our knowledge of the Paleoproterozoic biogeochemical process.

Salinity and redox conditions are intrinsic water mass properties that can provide insights into the geochemical evolution of ancient sedimentary environments over time (Wei and Algeo, 2020; Gilleaudeau et al., 2021; Song et al., 2021; Remírez et al., 2024). The temporal and spatial distribution patterns of these properties in the water column are associated with various factors, including watershed morphology, detrital input, connectivity with the open ocean, and other related processes (Algeo and Tribovillard, 2009; Zhang et al., 2017; Wei et al., 2018; Gilleaudeau et al., 2021). Thus, water mass properties such as density, salinity, redox state and temperature may relate closely to the formation of mineral resources, including Fe, manganese (Mn), and hydrocarbons, and is therefore of economic significance (e.g. Xu et al., 2015; Konhauser et al., 2017; Wei et al., 2024). Specifically, paleo-salinity and paleo-redox proxies may help link the evolution of the atmosphere, hydrosphere and biosphere to regional and global events (e.g. (Tribovillard et al., 2006; Konhauser et al., 2017; Wei and Algeo, 2020), such as the Great Oxidation Event (GOE) at ~2.5 billion years ago (Large et al., 2022).

This study investigates the paleoenvironmental evolution of the Minas Basin using geochemical and iron speciation analyses of Paleoproterozoic phyllites from the Gandarela Syncline, northeastern Quadrilátero Ferrífero, Brazil. The analyzed samples, deposited before and after the giant iron deposit (Cauê BIF), provide insights into paleoenvironmental reconstruction of the study area. The dynamic of paleosalinity and paleo-redox conditions influenced the geochemical cycles within the basin which contributed to iron ore genesis. Samples from three drill cores and outcrops were analyzed for paleosalinity proxies: boron (B)/ gallium (Ga), strontium (Sr)/ barium (Ba) and sulfur (S)/ total organic carbon (TOC), Fe speciation and RSE enrichment (e.g. molybdenum (Mo), nickel (Ni), uranium (U)). Although all proxies are likely affected by regional greenschist metamorphism (see below), the consistent trends in geochemical data can be interpreted as reflecting changes in the original seawater composition. The integrated geochemical data indicate a progressive transition from freshwater-brackish conditions during deposition of the Caraça Group to marine

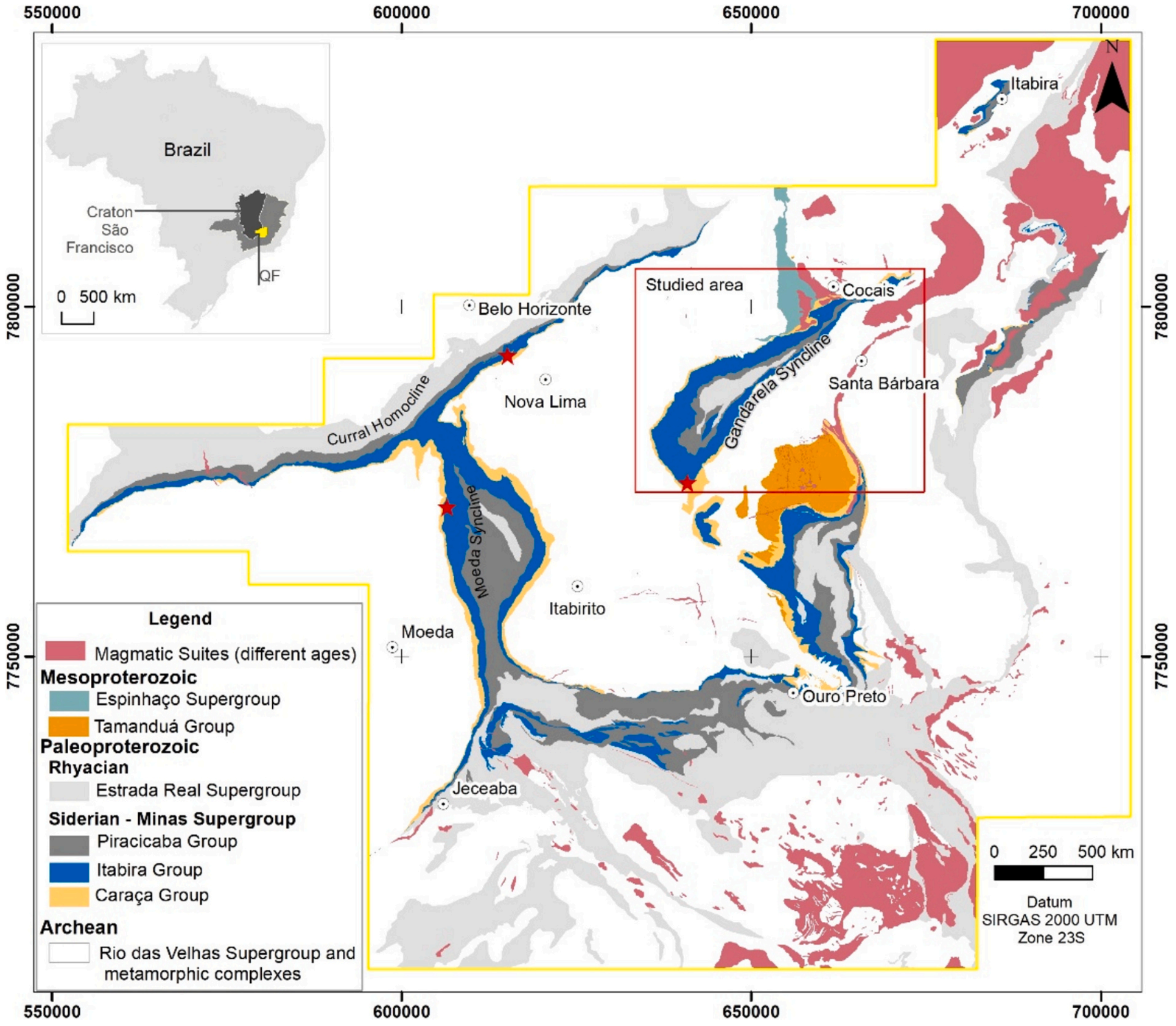

Fig. 1. Geological map of the Quadrilátero Ferrífero Province, with the inset showing the location of the São Francisco Craton within Brazil (modified from Endo et al., 2019 and Dutra et al., 2020). Additional symbols: red polygon: studied area, red stars: reference data, white circle, city's name. (For interpretation of the references to colour in this figure legend, the reader is referred to the web version of this article.)

facies (Itabira and Piracicaba groups) within a predominantly ferruginous, anoxic basin. These findings revise the previous model, that suggests marine facies were widely established in the Minas Basin during the early stages of BIF deposition.

2. Geologic background

The Quadrilátero Ferrífero province, which covers approximately 15,000 km^2, is situated within the São Francisco Craton in southeastern Brazil (Fig. 1). It is renowned for its world-class gold and iron deposits (Lobato et al., 2001; Rosière et al., 2008). Despite more than 80 years of iron mining, the giant Paleoproterozoic iron deposit, the Cauê BIF, still contains over 25 Gt, with an average grade of 43 % Fe, as reported resources (Vale, 2024). The present study is focused in the Gandarela area, which resides in the northeastern region of the Quadrilátero Ferrífero (Figs. 1 and 2). The area's structural framework is defined by the Gandarela syncline, a reclined fold with an NE-SW striking axial trace and an SE-plunging hinge line (Chemale Jr et al., 1994; Oliveira et al., 2010).

The study area is dominated by the Paleoproterozoic strata from the Minas Supergroup and our research focuses on the phyllite layers deposited before, and after, the Cauê BIF layer (~2.4 Ga) (Fig. 2). The metasedimentary rocks of the Minas Supergroup record repeating transgressions-regressions marine cycles in the Minas Basin (Dorr, 1969; Canuto, 2010; Gonçalves and Uhlein, 2022) and are classified into three units from the base to top, named the Caraça, Itabira and Piracicaba groups (Fig. 2), according to the subdivision proposed by Endo et al. (2019), Endo et al. (2020)), based on Dorr (1969). At the stratigraphic base, the Caraça Group is composed of conglomerate and quartzite overlain by phyllite, minor BIF and carbonate rocks, all of which are interpreted to reflect the depositional evolution from alluvial to fluvial, lacustrine and deltaic to marine environments (Dorr, 1969; Madeira et al., 2019; Gonçalves and Uhlein, 2022). Detrital zircon ^{207}Pb/^{206}Pb dates constrain the maximum sedimentation age for the Caraça Group to 2.5 Ga (Machado et al., 1996; Hartmann et al., 2006; Koglin et al., 2014; Nunes, 2016; Dopico et al., 2017; Rossignol et al., 2020). In the northeastern portion of the study area, some authors (e.g., Dorr, 1969; Endo et al., 2019) have distinguished the Tamanduá Group as the basal unit of the Minas Supergroup. However, its extent, timing, and stratigraphic context remain controversial (e.g. Simmons and Maxwell, 1961; Marshak and Alkmim, 1989; Daher et al., 2020; Dutra et al., 2020). In this study, basal fine-grained sedimentary rocks which were deposited earlier than the BIF from the Itabira Group, have been attributed to the Batatal Formation (Fig. 2) (e.g. Gonçalves and Uhlein, 2022).

The Itabira Group records chemical precipitation within a passive margin basin (Dorr, 1969; Alkmim and Marshak, 1998). At the base, the Cauê Formation features BIF deposition on the continental shelf (Klein and Ladeira, 2000). Overlying this, the Gandarela Formation comprises carbonate rock, including dolostone and limestone, locally stromatolitic, dolomitic BIF, and minor phyllite and intraformational breccia (Dorr, 1969; Souza and Müller, 1984; De Paula et al., 2023). The carbonate rocks were deposited in a shallow marine environment (Dorr, 1969; Babinski et al., 1995) within a tidal depositional system characterized by high-energy intertidal to shallow subtidal zones (Bekker et al., 2003). They were deposited ca. 2420 ± 19 Ma, according to a Pb/Pb whole rock isochron age dating of stromatolitic facies from the Gandarela Formation (Babinski et al., 1995). Furthermore, Cabral et al. (2012) obtained a U—Pb zircon age of 2655 ± 6 Ma for a purported meta-volcanic layer overlying the Cauê Formation, proposing an Archean age for it. However, this interpretation is contentious as it contradicts published detrital zircon data for the underlying Moeda Formation, which suggests a maximum depositional age of around 2.5 Ga and could represent an inherited population (Koglin et al., 2014; Farina et al., 2016; Nunes, 2016; Dopico et al., 2017).

The uppermost stratigraphic unit, the Piracicaba Group, consists of clastic sedimentary rocks (phyllite, quartzite and minor carbonates) interpreted to represent marine deposition (Dorr, 1969). Detrital zircon

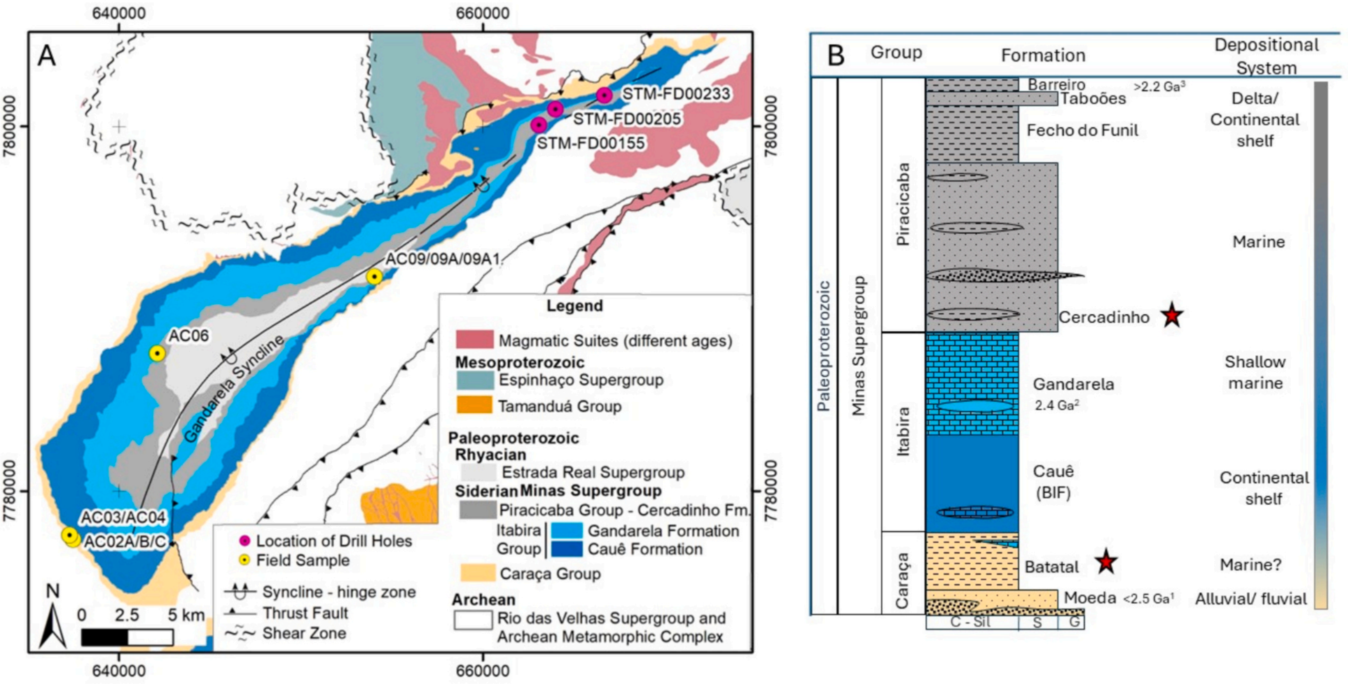

Fig. 2. (A) Geological map of Gandarela Syncline showing drill holes and field sample locations (modified from Endo et al., 2019 and Dutra et al., 2020). The outcrop locations GAD-SW includes AC02A, AC02B, AC02C, AC-03 and AC-04 samples; GAD-Central is associated with the AC06; and GAD-NE includes AC09, AC09A and AC09A1. Datum SIRGAS 2000 UTM - Zone 23S. (B) The stratigraphic column from Quadrilátero Ferrífero modified from Farina et al. (2016) and Endo et al. (2019). The lithostratigraphic unit are represented by the colours shown in (A), while the red stars indicate the studied stratigraphic units. Depositional ages are from [1]Koglin et al., 2014[2]Babinski et al. (1995) and [3] Machado et al. (1996). (For interpretation of the references to colour in this figure legend, the reader is referred to the web version of this article.)

$^{207}Pb/^{206}Pb$ dates constrain the maximum sedimentation age for the lowermost Cercadinho Formation to 2.6 Ga (Mendes et al., 2014; Dopico et al., 2017; Dutra et al., 2020). However, based on chemostratigraphy (Bekker et al., 2003) and a 2110 ± 10 Ma Pb—Pb carbonate whole rock isochron for the Fecho do Funil Formation (Babinski et al., 1995), the age of deposition of the Piracicaba Group could be younger than that, straddling the Rhyacian. The Quadrilátero Ferrífero Province underwent greenschist metamorphism associated with Rhyacian (2.2–2.0 Ga) and Ediacaran/Cambrian (Brasiliano, 570–480 Ma) orogenesis (Chemale Jr et al., 1994; Alkmim and Marshak, 1998; Oliveira et al., 2010; Seixas et al., 2013; Gonçalves-Dias et al., 2022).

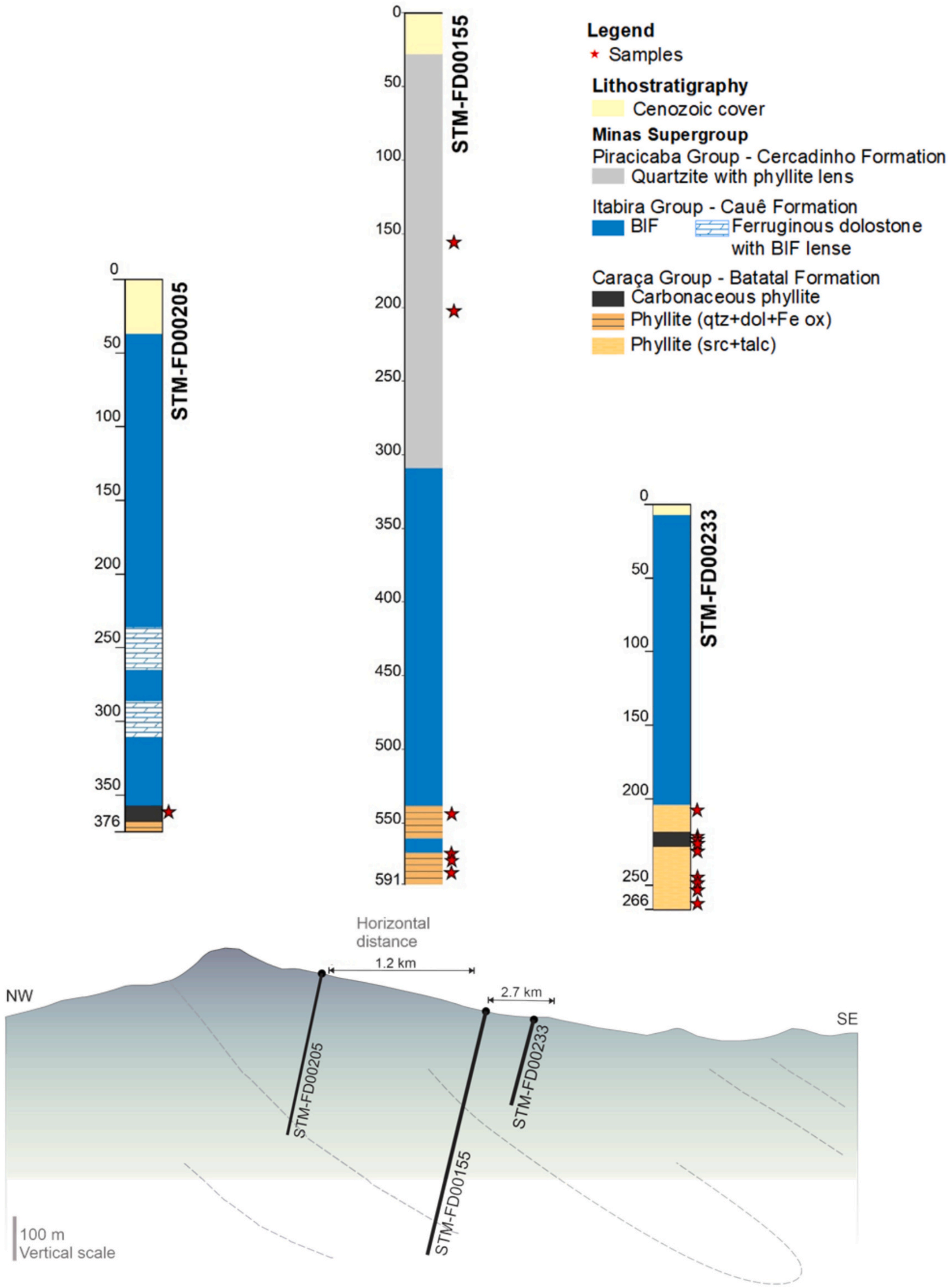

Fig. 3. (A) Stratigraphic column of drill holes *155, *205 and *233, aligned using the contact between the Cauê BIF and the Caraça phyllite as the horizontal datum. (B) Schematic vertical profile of the studied area.

3. Sampling and methods

3.1. Sample collection and mineralogy

We collected a total of 27 samples from the Gandarela syncline, divided into two sets to represent the Batatal and Cercadinho Formation (Fig. 2B). The first set comprises three drill cores obtained from the Serra do Tamanduá, situated in the northeastern part of the syncline (Fig. 2A). This set includes 19 phyllite samples, provided by the Vale S.A: STM-FD00155 (591 m deep), STM-FD00205 (376 m deep), and STM-FD00233 (266 m deep) (Fig. 3). The second set consists of 8 samples collected from well-preserved outcrops: GAD-SW, GAD-Central, and GAD-NE, each representing a different structural area within the Gandarela Syncline. GAD-SW is situated in the southwest, near the hinge zone; GAD-Central represents the normal flank in the central region; and GAD-NE is in the northeast, corresponding to the inverse flank of the syncline (Fig. 2). Rocks exhibiting evident hydrothermal alteration, such as carbonate and quartz veins, were excluded from analysis. From the selected samples, we obtained 27 elemental concentrations (major and trace elements), 12 TOC analyses, 7 X-ray diffraction (XRD) analyses of mineral composition and 19 results for Fe speciation.

Different stratigraphic levels of the Minas Supergroup were sampled. The lower stratigraphic unit comprises metasedimentary rocks from the Batatal Formation, representing the deposition before the Cauê BIF. The GAD-SW outcrop (Fig. 2) has nearly 200 m of sericitic phyllite. The upper stratigraphic unit is represented by the Cercadinho Formation, which records the deposition following the Cauê BIF and Gandarela dolostone. This unit contains quartz-rich, micaceous and ferruginous phyllites, along with fine-grained quartzite, which is exposed on both limbs of the Gandarela syncline (GAD-Central and GAD-NE) and was also observed in drill core STM-FD00155 (Fig. 3). The GAD-Central outcrop includes the sample AC06, while samples AC09, AC09A and AC09A1 were taken from the overturned flank (GAD-NE), near the bottom contact with the Cauê BIF (Fig. 2). The Cercadinho Formation reached a thickness of 280 m thick in the drill core, but its actual thicknesses may exceed 1000 m. No clastic interbeds were found within any of the studied sections of Cauê BIF and Gandarela dolostone.

The samples were characterized by X-ray diffraction (XRD) at the XRD Laboratory of the University of Alberta in Canada. The powdered samples were analyzed using a Bruker D8 Advance diffractometer with a cobalt radiation source ($\lambda = 1.78897$ Å) operated at 35 kV and 40 mA. Mineral phases were identified using DIFFRAC.EVA software (Bruker) and the PDF-4 database from the International Centre for Diffraction Data (ICDD).

3.2. Multi-elemental geochemistry

3.2.1. Major and trace elements

The geochemistry analyses were performed at SGS Geosol Laboratory Ltd., Belo Horizonte, Brazil. The samples were first dried at 100 °C, then pulverized to achieve 95 % <106 μm particle size. A 10 g portion of each sample was designated for either fusion or acid digestion. In the fusion method, the sample underwent lithium metaborate fusion at 950 °C, followed by the addition of a solution containing nitric and tartaric acids. In the acid digestion method, the samples were subjected to four acid digestion processes involving the combination of nitric, hydrochloric, hydrofluoric, and perchloric acids. Elemental content was measured using inductively coupled plasma-mass spectrometry (ICP-MS, model Agilent 7800/7850) or optical emission spectrometry (ICP-OES, model Agilent 5110 e 5800). The loss on ignition (LOI) values were determined by measuring the relative difference in mass after roasting at 1000 °C. Analytical errors are less than 5 % for most major oxides and 10 % and 15 % for most trace elements.

3.2.2. Boron analyses

Boron concentrations were analyzed in the Geobiology laboratory at the University of Alberta. Boron was extracted from these samples via partial digestion using concentrated aqua regia (a 3:1 mixture of hydrochloric and nitric acid). Then, 100 mg of dried and homogenized powder were weighed out and placed in a sterile 50 mL centrifuge tube, where 3 mL of 37 % HCl and 1 mL of 70 % HNO_3 were mixed into each sample and left to react at room temperature. After 1 h, each sample was remixed, placed in an aluminum block and heated to 130 °C for an additional 3 h. Each sample was left to cool at room temperature, and then diluted for analysis. The diluted solution was analyzed using an Agilent 8800 Triple Quadrupole ICP-MS/MS with a deviation of less than 5 %.

3.2.3. Organic carbon content

Total organic carbon analyses were conducted at the Natural Resources Analytical Laboratory, University of Alberta (Canada). Samples were weighed into open silver capsules and acidified through sequential additions of 50 μL of 1 M HCl to remove inorganic carbon. Subsequently, the samples were dried at 70 °C overnight, sealed and analyzed using a Thermo FLASH 2000 Organic Elemental Analyzer. During analysis, the samples were exposed to an extremely oxidizing environment, promoting an exothermic reaction responsible for the complete combustion of organic matter at temperatures reaching approximately 1800 °C. The resulting gases (N_2, CO_2, and H_2O) were separated using a chromatographic column, and the organic carbon content was quantified using a thermal conductivity detector. The analytical precision for TOC measurements was ±0.5 wt%.

3.3. Iron speciation

Iron speciation analyses were performed at the Sedimentary Geochemistry Laboratory, Stanford Doerr School of Sustainability, Stanford University, United States. The technique, as described by Poulton and Canfield (2005) and Alcott et al. (2020), quantifies the Fe contents in distinct phase pools that are highly reactive (Fe_{HR}) toward sulfide on early diagenetic timescales (Poulton and Canfield, 2005, 2011; Lyons and Severmann, 2006; Raiswell et al., 2018). Operationally defined phase pools include carbonate iron (Fe_{car}), ferric oxides (Fe_{ox}), magnetite (Fe_{mag}), pyrite (Fe_{py}), and unreactive silicate iron (Fe_U), whose concentrations are determined through a sequential reagent attack process. Highly reactive iron (Fe_{HR}) is calculated as the sum of the iron mineral phases: Fe_{car} (extracted using a 48-h sodium acetate reaction at 50 °C), Fe_{ox} (2-h sodium dithionite reaction at room temperature), Fe_{mag} (6-h ammonium oxalate reaction at room temperature) and Fe_{py} (chromium reduction of sulfur (CRS) method, Canfield et al., 1986). Iron contents in each sequential extraction pool were determined using the ferrozine spectrophotometric method (Stookey, 1970; with the colour allowed to develop overnight) and calculated through gravimetric measurements for Fe_{py}. Detailed methods and estimates of precision can be found in the Supplementary Material of Sperling et al. (2021). Total Fe contents used in the calculation of Fe_{HR}/Fe_T were obtained from SGS Geosol as described above. Fe_{HR}/Fe_T ratios are generally below 0.22 for samples deposited under oxic bottom water conditions, and above 0.38 for anoxic bottom waters, with ambiguous samples plotting in between (Raiswell et al., 2018). The Fe_{py}/Fe_{HR} ratio further allows for the distinction of anoxic samples, which may have been deposited under ferruginous (nonsulfidic) or euxinic (anoxic with free sulfide) conditions, with a threshold of about 0.7 (März et al., 2008). Pasquier et al. (2022) challenged these proxy thresholds; however, the compilation used by the authors included a number of samples inappropriate for iron speciation according to Raiswell et al. (2018) criteria. Several caveats exist for iron speciation in ancient and metamorphosed rocks (see Raiswell et al., 2018; Slotznick et al., 2018) and these are discussed further below.

4. Results

4.1. Petrological and petrographic observations

The basal unit of the Batatal Formation is primarily composed of phyllites, with minor occurrences of dolomitic BIF (Fig. 3). The GAD-SW outcrop is composed of a dark gray, fine-grained sericite-phyllite, mainly consisting of sericite, quartz, minor muscovite, organic matter, and rutile (Fig. 4A). These phyllites are lepidoblastic and display both laminated and non-laminated structures (Fig. 4B). Samples from the drill hole STM-FD00155 presented secondary crystals of magnetite, pyrite, carbonate, and quartz overgrowing the foliation. In contrast, the fine-grained metasiliciclastic rocks of the Batatal Formation observed in the drill cores show significant compositional variations, ranging from chloritic, micaceous, and ferruginous to dolomitic phyllites, which may or may not contain organic matter. Accessory minerals include pyrite, rutile, and apatite. A specific occurrence of carbonaceous phyllite (Fig. 4C), which is less than 3 m thick, is identified in this unit. This rock is characterized by alternating organic matter-rich layers and rhythmic dolomite-quartz laminae, with secondary dolomite and quartz veining, shear zones, and intrafolial folds also present.

The upper layer of the Cercadinho Formation is predominantly fine-grained quartzite, which may be ferruginous and interbedded with phyllite (Fig. 3). The phyllite, which is the focus of this study, varies from white or silver to reddish in colour and is composed of quartz, sericite and muscovite, with minor Fe-oxide, kaolinite, and rare occurrences of plagioclase, serpentine, and talc. Toward the lower contact, the quartzite becomes iron-rich. Common structures include compositional laminae, pervasive schistosity, banding, intrafolial folds, and shear zones.

4.2. Geochemistry

4.2.1. Major elements

Whole-rock major oxide and trace element geochemical analyses were conducted on twenty-seven samples (Tables 1 and 2). Compositional variation of major elements in the phyllites of the Batatal Formation are shown in Table 1 and Fig. 5. The drill core samples display median values (range) of 17.7 wt% (11.3–24.1 wt%) for Al_2O_3, 0.7 wt% (0.2–3.4 wt%) for CaO, 7.8 wt% (2.3–18.7 wt%) for Fe_2O_3, 3.1 wt% (0.5–4.3 wt%) for K_2O and 57.1 wt% (47.0–72.0 wt%) for SiO_2. In contrast, phyllites in the southwest area (GAD-SW) are more compositionally homogeneous, with Al_2O_3 ranging from 21.3 to 33.9 wt%, CaO $<$ 0.12 wt%, Fe_2O_3 $<$ 5.6 wt%, SiO_2 between 44.0 and 65.2 wt%. Additionally, K_2O concentrations are notably higher in the southwest, ranging from 6.5 to 9.7 wt%. The variation in LOI is similar for both, ranging from 2.9 to 12.4 wt%.

The upper stratigraphic unit, the Cercadinho Formation, displays a wider compositional range (Fig. 5), which can be divided into two groups. The first group, represented by the ferruginous phyllite ($n = 3$), is characterized by elevated concentrations of Al_2O_3 (~25 wt%), Fe_2O_3 (11.6–14.6 wt%) and K_2O (4.8–6.7 wt%). In contrast, the second group consists of quartz-rich phyllite ($n = 2$), which is dominated by SiO_2 (~80.5 wt%) and lower contents of Fe_2O_3 (2.9 and 8.7 wt%), Al_2O_3 (<2.7 wt%), and K_2O (<0.7 wt%).

4.2.2. Redox-sensitive proxies

The trace metal abundances of analyzed phyllite samples are presented in Table 2. To quantify the authigenic enrichment of Cu, Ni, Mo, U and V in the rocks, the elemental concentrations in the samples were compared to the average composition of the Post-Archean Australian Shale (PAAS) (Taylor and McLennan, 1985; Tribovillard et al., 2006). The enrichment factor (EF) was calculated using the formula: $EF_{\text{element X}} = (X/Al)_{\text{sample}} / (X/Al)_{\text{PAAS}}$, where X represents the RSE element (e.g.

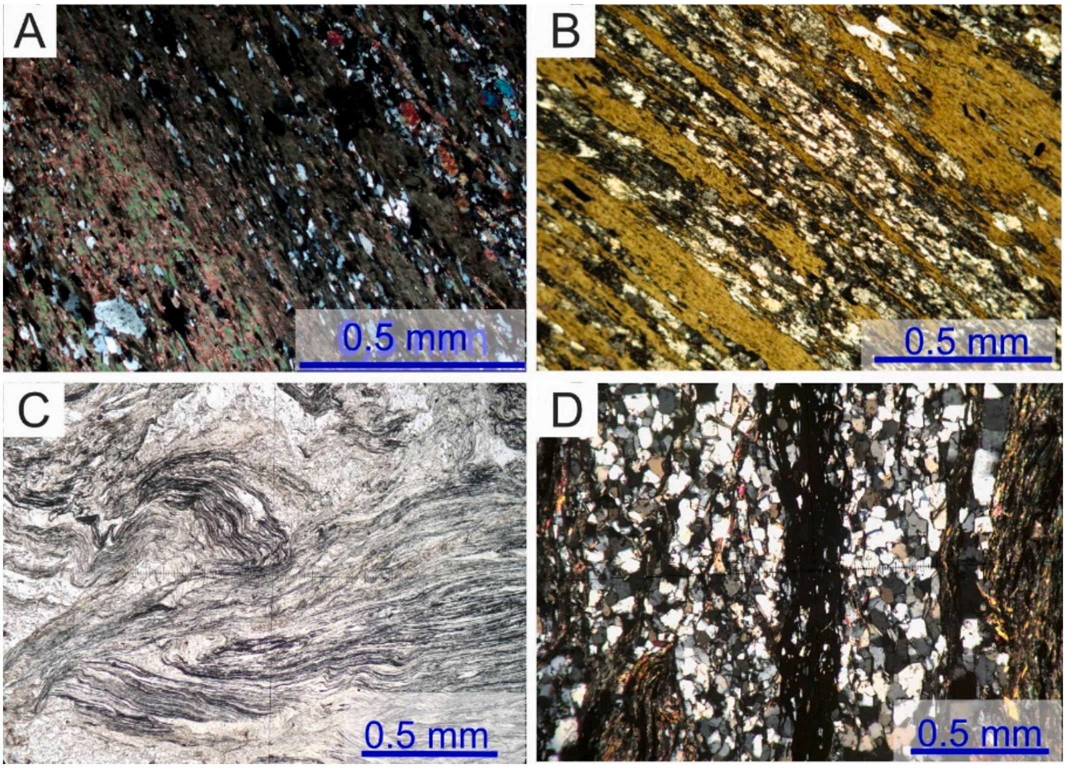

Fig. 4. Photomicrography. (A) Dolomitic phyllite with quartz laminae (*155-29B) in contact with dolomitic phyllite under crossed polarized light (XPL). (B) Chloritic phyllite finely laminated with quartz (XPL). (C) Carbonaceous phyllite from sample *233-A10 showing the organic matter layers (black) under parallel polarized light (PPL). (D) The same sample displaying the compositional variations in the carbonaceous phyllite (XPL).

Table 1

Chemical analyses of phyllite samples from the Gandarela syncline. Reference: 1, AC06; 2, AC09; 3, AC09A1; 4, *155-A001; 5, *155-A004; 6, AC02A; 7, AC02B; 8, AC02C; 9, AC03; 10, AC04; 11, *155-A019; 12, *155-A024; 13, *155-A025; 14, *155-A029B; 15, *205-A024; 6, *233-A006; 17, *233-A009; 18, *233-A010–06; 19, *233-A010–17; 20, *233-A010–22; 21, *233-A010–26; 22, *233-A010–29; 23, *233-A011; 24, *233-A012; 25, *233-A013; 26, *233-A014; 27, *233-A016. *Prefix of drill hole identification: STM-FD00.

	Cercadinho Formation			Batatal Formation SW			Batatal Formation NE																				
	1	2	3	4	5	6	7	8	9	10	11	12	13	14	15	16	17	18	19	20	21	22	23	24	25	26	27
Major Elements (%)																											
SiO_2	45.3	47.2	49.7	78.7	82.4	44.0	44.9	45.9	64.0	65.2	67.8	48.1	57.6	47.0	49.2	72.0	60.0	62.8	57.1	61.4	59.4	56.7	54.2	52.8	54.6	58.4	53.4
Al_2O_3	25.0	24.9	25.3	2.7	2.3	32.4	33.3	33.9	21.3	21.7	17.0	13.7	17.7	14.4	11.8	11.3	19.2	15.8	21.1	20.6	19.7	21.8	24.1	14.1	18.9	15.7	19.0
Fe_2O_3	14.6	13.5	11.6	8.7	2.9	5.6	2.1	2.0	1.7	1.6	2.3	18.0	7.8	14.0	17.7	5.5	8.5	7.1	6.0	5.9	6.8	6.9	6.8	18.7	8.8	12.9	10.7
K_2O	6.7	4.8	5.2	0.7	0.5	9.0	9.7	9.7	6.5	6.6	4.0	0.5	3.8	3.4	3.1	4.3	3.8	3.0	4.2	3.9	2.6	2.7	3.0	0.6	3.0	1.3	3.3
LOI	3.8	4.4	4.6	0.3	0.1	5.6	5.2	5.7	3.6	3.5	5.7	7.6	4.9	4.4	12.4	2.9	5.0	5.1	5.4	4.8	4.2	4.3	4.6	4.3	4.8	3.7	4.7
MgO	0.6	0.3	0.3	0.0	0.0	1.1	1.1	1.0	1.0	0.8	2.2	9.9	5.8	7.3	3.9	1.2	4.0	3.5	3.3	3.4	3.6	3.5	3.4	4.9	5.1	4.6	5.6
CaO	0.4	0.2	0.1	0.0	0.0	0.1	0.1	0.1	0.1	0.1	2.5	2.7	1.1	3.4	1.4	1.0	1.1	0.4	0.2	0.3	0.6	0.3	0.3	0.5	1.4	0.4	0.7
Na_2O	1.9	1.6	1.4	0.1	0.0	0.5	0.5	0.4	0.1	0.2	0.6	<0.01	0.2	3.4	0.2	0.1	0.5	0.5	0.9	0.9	1.3	1.6	1.9	1.1	2.3	2.2	0.6
TiO_2	0.9	0.7	0.8	0.1	0.2	1.0	1.1	1.1	0.7	0.7	0.2	2.8	0.7	2.8	1.4	0.3	0.7	0.6	0.7	0.7	0.7	0.8	0.9	0.5	0.7	0.5	0.6
P_2O_5	0.2	0.1	0.1	<0.01	<0.01	0.1	0.1	0.1	0.0	0.0	0.1	0.5	0.1	0.4	0.1	0.1	0.1	0.1	0.1	0.1	0.1	0.1	0.1	0.1	0.2	0.1	0.1
MnO	0.0	0.0	<0.01	<0.01	<0.01	0.0	<0.01	<0.01	<0.01	<0.01	0.0	0.1	0.1	0.1	0.6	0.0	0.1	0.1	0.0	0.1	0.1	0.1	0.1	0.1	0.1	0.1	0.1
N	0.06	0.08	0.08	0.07	0.08	0.12	0.12	0.13	0.09	–	–	0.09	–	–	–	–	–	0.10	–	–	–	–	–	–	–	–	0.07
C	0.04	0.04	0.03	0.05	0.04	0.75	0.66	0.69	0.47	–	–	0.88	–	–	–	–	–	2.79	–	–	–	–	–	–	–	–	0.37
TOC	0.04	0.03	0.03	0.04	0.02	0.47	0.51	0.67	0.42	–	–	0.16	–	–	–	–	–	2.61	–	–	–	–	–	–	–	–	0.32
S	<0.01	<0.01	<0.01	<0.01	<0.01	<0.01	<0.01	<0.01	<0.01	<0.01	0.02	<0.01	<0.01	0.81	1.69	0.09	0.11	0.66	0.34	0.26	0.13	0.13	0.14	0.02	0.07	<0.01	<0.01
Trace Elements (ppm)																											
B	25	22	37	24	22	63	72	70	47	–	–	21	–	–	–	–	–	31	–	–	–	–	–	–	–	–	26
Ba	1249	637	809	128	95	481	545	563	305	368	339	94	1327	255	164	1004	480	551	750	688	445	486	535	114	468	274	366
Cd	0	0	0	0	0	0	0	0	0	0	0	0	0	0	0	0	0	16	1	4	1	0	0	0	0	0	0
Co	3	3	2	1	1	37	2	7	1	2	2	45	30	76	20	4	34	58	57	47	35	42	40	37	43	41	47
Cr	119	92	81	54	13	114	87	67	51	54	1	23	86	52	83	4	147	172	177	147	125	120	138	199	191	207	266
Cs	3	6	5	<0.05	0	15	15	16	11	10	3	0	1	31	2	3	3	3	4	4	3	3	3	1	3	2	4
Cu	3	3	13	3	4	32	12	42	8	13	3	5	4	102	262	17	73	534	216	141	78	85	102	7	64	7	19
Ga	37	31	32	5	4	38	39	36	27	28	19	22	22	19	15	19	23	43	51	39	27	28	30	20	24	20	24
Hf	4	3	4	3	3	4	4	4	3	4	2	2	3	1	4	4	3	3	4	4	3	4	4	2	2	2	2
Mo	0	0	0	0	0	3	1	2	2	2	1	1	2	1	2	0	2	3	4	3	2	2	3	1	2	2	2
Nb	23	11	17	3	3	18	21	21	10	13	5	15	10	13	10	17	10	10	12	15	9	13	13	6	10	7	7
Ni	36	52	38	7	8	178	50	66	27	39	6	37	81	66	65	6	198	376	331	259	161	189	160	246	281	288	359
Pb	22	43	41	8	5	32	65	58	11	32	9	2	3	3	10	9	17	95	36	143	30	30	32	7	48	14	22
Rb	185	144	159	20	17	252	280	262	205	210	165	12	60	218	66	104	85	90	139	124	67	78	81	13	97	38	79
Sc	10	7	11	3	3	21	18	17	16	15	2	27	13	35	13	4	11	12	13	13	12	14	14	18	16	16	17
Sr	218	398	322	74	48	54	59	48	27	34	39	42	49	116	10	37	75	68	90	94	134	152	184	40	88	58	63
Ta	2	1	2	<0.05	<0.05	2	2	2	0	1	1	1	1	0	0	2	1	1	1	1	1	1	1	1	1	1	1
Th	18	16	21	5	4	25	33	32	17	22	5	2	13	1	9	11	11	10	12	14	10	13	13	8	10	7	8
U	3	3	4	2	1	5	5	5	3	6	4	1	4	0	3	2	3	3	4	4	3	4	4	2	3	2	2
V	218	148	786	61	29	212	457	335	136	160	LD	384	159	441	165	30	168	157	283	174	155	269	194	148	247	183	170
W	<0.1	1	<0.1	6	3	5	5	<0.1	4	2	2	1	5	3	4	<0.1	2	<0.1	2	2	2	3	<0.1	<0.1	4	<0.1	0
Zr	237	119	221	172	159	164	201	193	156	150	96	208	140	168	179	298	156	144	190	206	138	178	192	105	151	103	116

Table 2

Trace metal elements and relevant ratios for samples from the Gandarela syncline. Reference: 1, AC06; 2, AC09; 3, AC09A1; 4, *155-A001; 5, *155-A004; 6, AC02A; 7, AC02B; 8, AC02C; 9, AC03; 10, AC04; 11, *155-A019; 12, *155-A024; 13, *155-A025; 14, *155-A029B; 15, *205-A024; 6, *233-A006; 17, *233-A009; 18, *233-A010–06; 19, *233-A010–17; 20, *233-A010–22; 21, *233-A010–26; 22, *233-A010–29; 23, *233-A011; 24, *233-A012; 25, *233-A013; 26, *233-A014; 27, *233-A016. *Prefix of drill hole identification: STM-FD00.

	Cercadinho Formation					Batatal Formation SW					Batatal Formation NE															
	1	2	3	4	5	6	7	8	9	10	11	12	13	14	15	16	17	18	19	20	21	22	23	24	25	26	27
Rare Earth Elements + Y																											
La	125.6	53.4	80.3	11.0	10.0	74.1	123.7	120.6	47.9	66.9	14.3	21.7	32.8	14.9	22.2	56.1	34.8	31.7	42.1	44.6	35.5	42.4	43.6	24.7	34.7	25.6	29.0
Ce	185.2	94.7	146.2	21.6	18.3	134.6	236.6	238.4	86.5	126.7	26.3	51.2	62.9	35.3	44.7	117.3	65.5	59.7	82.9	85.7	66.7	73.4	81.7	47.1	63.3	45.6	54.7
Pr	29.1	10.0	15.1	2.4	2.1	13.3	25.6	25.1	9.6	13.2	2.9	6.9	7.1	5.0	5.4	13.5	6.6	6.6	11.0	9.5	7.4	7.7	8.9	5.2	7.0	5.2	5.7
Nd	105.0	36.3	55.7	9.1	7.9	47.8	95.2	92.6	33.7	51.5	11.1	33.4	26.1	23.1	22.2	54.3	26.6	24.9	38.9	34.4	25.4	29.3	33.2	20.0	25.2	17.7	22.9
Sm	20.4	6.1	8.8	2.0	1.4	7.7	16.1	14.4	6.3	9.0	2.0	8.5	5.3	6.5	4.9	10.3	4.5	4.6	4.4	5.1	4.3	5.2	5.9	3.2	4.0	2.6	3.2
Eu	4.1	1.3	1.9	0.4	0.3	1.8	2.7	3.7	1.2	2.1	0.6	2.4	1.8	2.3	1.1	1.2	1.0	1.0	0.8	1.1	0.9	1.2	1.3	1.2	1.2	0.8	0.9
Gd	17.8	4.5	9.4	2.1	1.5	6.8	11.4	12.7	4.7	7.3	2.0	9.6	4.9	7.1	5.2	11.2	3.8	3.9	5.1	5.7	4.2	5.1	5.2	3.1	3.8	2.5	3.8
Tb	2.6	0.9	1.4	0.4	0.3	1.2	1.9	1.8	0.8	1.1	0.3	1.4	0.8	1.1	0.9	2.0	0.7	0.7	0.9	1.0	0.8	0.8	0.9	0.6	0.8	0.6	0.8
Dy	13.0	5.2	8.5	2.3	1.8	7.0	9.3	9.0	4.7	5.2	1.3	7.8	4.2	6.7	5.3	12.0	4.2	4.3	4.7	6.1	4.3	5.0	5.0	3.6	4.4	3.2	3.9
Ho	2.6	1.1	1.6	0.5	0.4	1.5	1.7	1.7	0.9	1.0	0.3	1.7	0.9	1.3	1.1	2.5	0.8	0.8	1.1	1.2	0.9	1.0	0.8	0.7	0.9	0.7	0.7
Y	69.1	28.6	44.7	14.4	12.7	39.7	47.4	45.5	22.6	29.1	7.7	43.8	25.1	36.8	33.5	66.4	24.4	22.4	28.3	35.5	25.5	29.1	25.3	18.1	24.6	17.1	20.0
Er	6.9	2.9	4.5	1.6	1.3	3.8	5.0	5.4	2.5	3.0	0.8	4.5	2.5	3.9	3.7	6.9	2.1	1.9	2.8	3.2	2.2	2.9	2.5	1.6	2.3	2.1	1.9
Tm	1.1	0.5	0.7	0.2	0.2	0.5	0.7	0.7	0.4	0.5	0.1	0.6	0.3	0.5	0.5	1.1	0.4	0.3	0.5	0.5	0.3	0.4	0.5	0.3	0.4	0.3	0.3
Yb	5.7	2.9	4.6	1.7	1.3	3.9	4.3	3.9	2.8	2.8	0.8	4.2	2.4	3.3	3.6	6.5	2.2	2.2	2.7	3.1	2.3	2.7	2.7	1.5	2.2	1.8	1.8
Lu	0.6	0.2	0.4	0.3	0.2	0.5	0.6	0.7	0.4	0.5	0.3	0.8	0.4	1.0	0.7	1.0	0.4	0.4	0.6	0.4	0.2	0.4	0.4	0.3	0.4	0.4	0.3
Relevant Ratios																											
B/Ga	0.7	0.7	1.1	4.5	5.6	1.6	1.8	1.9	1.8	–	–	0.9	–	–	–	–	–	0.7	–	–	–	–	–	–	–	–	1.1
S/TOC	0.3	0.3	0.3	0.3	0.4	0.0	0.0	0.0	0.0	–	–	0.1	–	–	–	–	–	0.3	–	–	–	–	–	–	–	–	0.0
Sr/Ba	0.2	0.6	0.4	0.6	0.5	0.1	0.1	0.1	0.1	0.1	0.1	0.5	0.0	0.5	0.1	0.0	0.2	0.1	0.1	0.1	0.3	0.3	0.3	0.3	0.2	0.2	0.2
Cr_{EF}	1.4	1.2	0.8	3.0	0.9	1.1	0.8	0.7	0.7	0.7	0.0	0.3	1.2	0.6	1.6	0.1	2.4	3.0	2.7	2.1	2.0	1.9	1.9	2.5	2.6	2.8	3.0
Cu_{EF}	0.1	0.1	0.2	0.2	0.4	0.4	0.2	0.6	0.1	0.2	0.1	0.1	0.1	1.7	6.8	0.4	1.6	12.4	4.5	2.7	1.7	1.8	1.8	0.1	1.2	0.1	0.3
Mo_{EF}	0.4	0.5	0.2	2.3	2.0	2.8	1.0	2.4	2.6	3.0	1.0	1.3	2.1	0.8	4.2	0.8	3.5	6.1	6.4	4.6	3.5	3.6	3.4	1.7	2.5	2.1	2.0
Ni_{EF}	0.7	1.1	0.6	0.6	0.9	2.8	0.8	1.2	0.6	0.9	0.1	0.9	1.8	1.4	2.1	0.2	5.3	10.9	8.6	6.2	4.3	5.0	3.6	5.1	6.3	6.4	6.8
U_{EF}	3.5	4.7	4.1	11.6	9.3	4.7	5.0	5.9	3.9	8.5	6.2	0.9	6.2	0.6	6.7	3.9	5.7	5.5	6.3	6.1	4.8	6.2	5.6	2.7	4.2	2.6	2.7
V_{EF}	1.8	1.3	5.3	2.4	1.4	1.4	3.2	2.7	1.3	1.5		3.9	1.5	3.9	2.3	0.4	1.9	2.0	3.1	1.8	1.8	3.0	1.9	1.3	2.4	1.7	1.4
Zn_{EF}	0.1	0.1	0.1	0.3	0.7	0.2	0.1	0.1	0.2	0.2	0.3	2.9	1.0	1.4	0.5	1.2	2.7	104.8	3.9	10.6	7.5	4.6	5.0	2.8	1.8	1.9	1.5
Mo_{EF}/U_{EF}	0.1	0.1	0.1	0.2	0.2	0.6	0.2	0.4	0.7	0.4	0.2	1.4	0.3	1.4	0.6	0.2	0.6	1.1	1.0	0.7	0.7	0.6	0.6	0.6	0.6	0.8	0.7
Fe/Al	1.4	1.4	0.9	4.0	1.6	0.4	0.2	0.2	0.2	0.2	0.3	2.1	0.9	1.4	2.9	0.9	1.1	1.0	0.8	0.7	0.9	0.9	0.8	1.9	1.0	1.4	1.0
Y/Ho	26.6	26.5	28.3	29.9	31.7	27.4	28.7	26.3	25.1	28.5	28.6	26.4	28.9	28.3	29.4	26.3	31.7	27.0	26.2	30.3	28.3	29.1	31.6	26.6	28.6	24.5	28.9
C_{org}/P	1.2	1.4	0.7	7.0	–	12.5	14.4	19.7	37.8	–	–	0.8	–	–	–	–	–	97.9	–	–	–	–	–	–	–	–	10.8

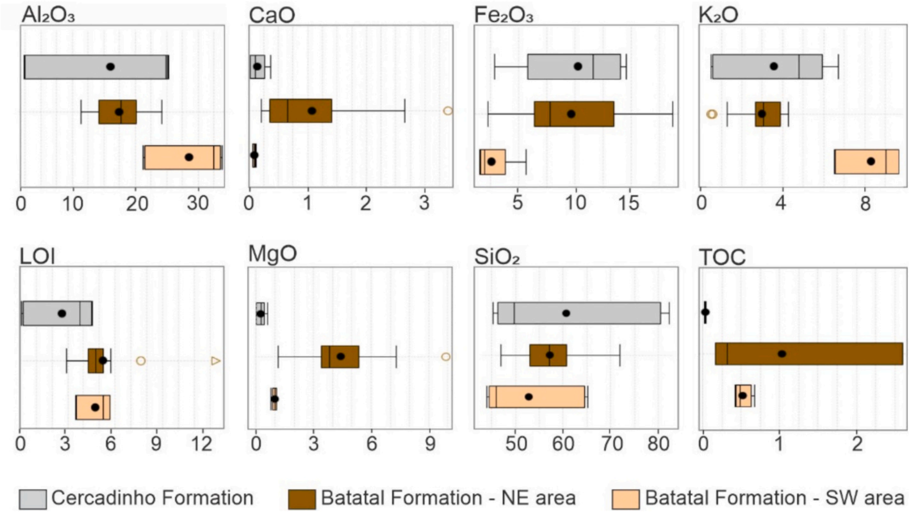

Fig. 5. Box plot representing the major elements in the phyllite from different stratigraphic layers. Boxes represent 25 % and 75 % of the data from each core, with the median value for each parameter shown within the box and the full range of data bracketed above and below the box.

Mo and U) and Al represents the aluminum abundance (Tribovillard et al., 2006).

The lower stratigraphic phyllites of the Batatal Formation exhibit significant enrichment in RSE, such as Cr_{EF}, Cu_{EF}, Ni_{EF} and Zn_{EF}, as well as elevated Mo_{EF}/U_{EF} ratios (Figs. 6 and 9). Drill core samples from the northeastern extremity of the study area reveal elevated RSE concentrations, with median values of Cr at 138 ppm (range 1–266 ppm), Cu at 73 ppm (range 3–534 ppm), Ni at 189 ppm (range 6–376 ppm), and Zn at 135 ppm (range 17–4821 ppm) where the EF values range as follows (median values) Cr_{EF}, 0.01–3.0 (2); Cu_{EF}, 0.1–12.4 (1.6); Mo_{EF}, 0.7–6.4 (2.5) Ni_{EF}, 0.2–10.9 (5), and Zn_{EF}, 0.3–104.8 (2.7). The Mo_{EF}/U_{EF} ratio has a median of 0.6 (range 0.2–1.4). The highest RSE

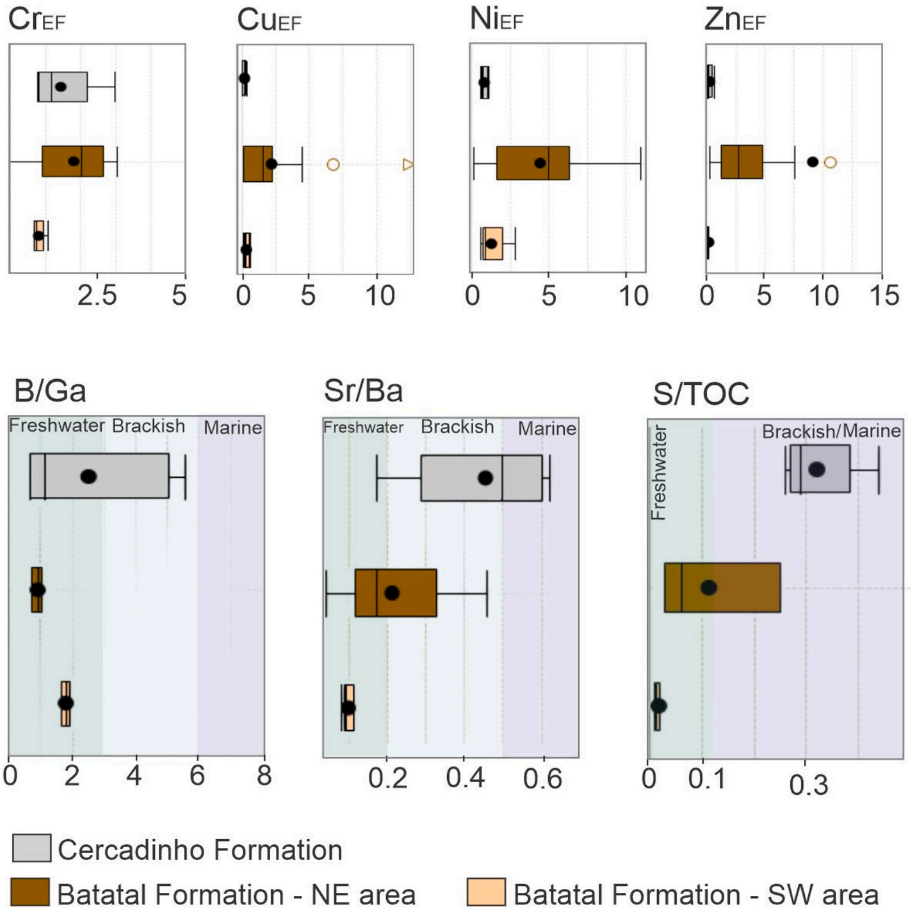

Fig. 6. Box plot representing the trace metal enrichment factor in the phyllite from different stratigraphic layers. Boxes represent 25 % and 75 % of the data from each core, with the median value for each parameter shown within the box and the full range of data bracketed above and below the box. The Zn_{EF} outlier = 104 is not plotted to represent the range better.

concentrations are primarily associated with carbonaceous phyllite.

In contrast, the southwestern region (GAD-SW) of the Batatal phyllites shows lower RSE concentrations when compared to the northeastern area (Figs. 6 and 9). The median (range) values for Cr, Cu, Mo, Ni and Zn are 67 ppm (51–114 ppm), 13 ppm (8–42 ppm), 2 ppm (1–3 ppm), 50 ppm (27–178 ppm), and 12 ppm (10–20 ppm), respectively. The EF values show the following range (median): Cr_{EF}, 0.7–1.1 (0.7); Cu_{EF}, 0.1–0.6 (0.2); Mo_{EF} 0.1–3.0 (2.6); Ni_{EF}, 0.6–2.8 (0.9), and Zn_{EF}, 0.1–0.2 (0.2). The Mo_{EF}/U_{EF} ratio has a median of 0.4 (range: 0.2 to 0.7), while the C_{org}/P ratio varies from 12.5 to 37.8, with a median of 17.1.

In the younger stratigraphic unit, the Cercadinho Formation, trace metal abundance decreases (Figs. 6 and 9). Chromium, Cu, Mo, Ni and Zn show a median (range) are: 81 ppm (13–119 ppm); 3.4 ppm (2.9–12.6 ppm); 0.4 ppm (0.2–0.4 ppm), 36 ppm (7–52 ppm) and 8 ppm (5–9 ppm), respectively. In general, the EF values represent the lower enrichment levels observed in the studied samples and are expressed as ranges (median): Cr_{EF}, 0.7–3.0 (1.2); Cu_{EF}, 0.05–0.4 (0.2); Mo_{EF} 0.2–2.3 (0.5); Ni_{EF}, 0.6–1.1 (0.7), and Zn_{EF}, 0.1–0.7 (0.1). The Mo_{EF}/U_{EF} ratio ranges from 0.1 to 0.2, with a median of 0.12. C_{org}/P ratios range from 0.72 to 6.96, with a median of 1.3.

4.2.3. *Paleosalinity proxies*

Elemental paleosalinity proxies expressed by the relative concentration of B/Ga, Sr/Ba and S/TOC were analyzed in the studied samples. Because Sr can substitute for Ca^{2+} in carbonates, and thus record the presence of carbonate rather than a paleosalinity signal in Sr/Ba proxy reconstructions, all studied samples contain <5 wt% CaO in carbonate content (Brand and Veizer, 1980; Wei and Algeo, 2020).

B/Ga values increase upwards in the stratigraphic section (Fig. 6). At the base, Batatal phyllite samples from the GAD-SW, southwestern area, show a median value of 0.9 (range: 0.7–1.1). This value rises in the northeastern region, where the median B/Ga reaches 1.8 (range: 1.6–1.9). In contrast, the upper stratigraphic unit, represented by the Cercadinho phyllite, exhibits a wider range of B/Ga values, from 0.7 to 5.6, with a median of 1.1.

The Sr/Ba ratio in the Batatal samples from the GAD-SW outcrop ranges from 0.08 to 0.11, with a median of 0.09. In the northeastern region, the Batatal phyllites show greater variability, with Sr/Ba values between 0.04 and 0.46 and a median of 0.17 (Fig. 6). Conversely, samples from the uppermost stratigraphic unit, the Cercadinho Formation, reveal the highest Sr/Ba values, with a maximum of 0.62, with a median of 0.50 and minimum of 0.17 (Fig. 6).

Regarding S/TOC ratios, all analyzed phyllite samples from the Batatal and Cercadinho formations show low S concentrations, ranging from 0.01 wt% to 0.26 wt%, except the Batatal carbonaceous phyllite (e.g., samples STM-FD00155-A29B, STM-FD00205-A24, STM-FD00205-A10–06, and STM-FD00233-A10–17), where S concentration reaches up to 1.69 wt%. Consequently, the Batatal phyllites exhibit S/TOC values ranging from 0.01 to 0.25, with a median of 0.02. In contrast, the Cercadinho Formation, which corresponds to the upper stratigraphy, displays higher S/TOC values, ranging from 0.3 to 0.4, with a median of 0.3.

4.3. *Iron speciation*

In the studied stratigraphic section, unreactive iron (Fe_U) is the predominant phase across all samples, with concentrations ranging from 0.77 to 8.85 wt% (Table 3). In contrast, the abundance of highly reactive iron (Fe_{HR}), which includes the Fe-oxide, Fe-carbonate, magnetite and pyrite pools, varies from 0.13 to 2.0 wt% (Fig. 7).

In the lower unit, consisting of phyllite from the Batatal Formation in the southwestern area (GAD-SW outcrop), the ratio of Fe_{HR} to total iron (Fe_T) ratio ranges from 0.29 to 0.46, with a median of 0.37. The Fe_{Py}/Fe_{HR} ratio is zero, indicating an absence of Fe_{Py} in the rocks. Conversely, the Batatal Formation in the northeastern area displays greater variability, with Fe_{HR}/Fe_T values ranging from 0.01 to 0.49, and a median of

Table 3
Sequential iron extraction data.

Sample	Lithostatigraphy	Fe_{carb} (wt %)	Fe_{ox} (wt %)	Fe_{mag} (wt %)	Fe_{Py} (wt %)	Fe_{HR} (wt %)	Fe_U (wt %)	Fe_T (wt %)	Fe_{Py}/Fe_{HR}	Fe_{HR}/Fe_T	Fe/Al
AC06		0.01	0.96	0.02	0.00	0.99	9.20	10.19	0.00	0.10	1.44
AC09		0.02	1.48	0.05	0.00	1.55	7.91	9.46	0.00	0.16	1.43
AC09A		0.01	1.84	0.04	0.00	1.90	16.56	18.46	0.00	0.10	6.26
AC09A1		0.01	1.06	0.02	0.00	1.09	7.00	8.09	0.00	0.14	0.91
STM-FD00155-A01		0.02	0.99	0.02	0.00	1.03	5.06	6.09	0.00	0.17	3.98
STM-FD00155-A04	Cercadinho Formation	0.01	0.11	0.01	0.00	0.13	1.91	2.04	0.00	0.06	1.64
AC02A		0.03	1.75	0.02	0.00	1.80	2.14	3.94	0.00	0.46	0.44
AC02B		0.06	0.48	0.04	0.00	0.59	0.88	1.47	0.00	0.40	0.17
AC02C	Batatal Formation - SW area	0.03	0.36	0.02	0.00	0.41	1.01	1.42	0.00	0.29	0.19
AC03		0.03	0.34	0.04	0.00	0.41	0.77	1.17	0.00	0.35	0.19
STM-FD0015-A19		0.31	0.01	0.01	0.00	0.32	1.30	1.62	0.00	0.20	0.28
STM-FD00155-A24		0.78	0.03	0.15	0.00	0.96	11.66	12.62	0.00	0.08	2.14
STM-FD00155-A25		0.10	0.01	0.03	0.00	0.14	5.33	5.47	0.00	0.02	0.88
STM-FD00233-A06		0.78	0.09	0.04	0.08	0.99	2.87	3.85	0.08	0.26	0.89
STM-FD00233 A010–06		0.41	0.11	0.12	0.33	0.97	4.00	4.97	0.34	0.19	1.03
STM-FD00233 A010–08*		0.20	0.06	0.08	0.42	0.76	3.82	4.58	0.55	0.17	0.89
STM-FD00233 A010–17		1.07	0.23	0.24	0.33	1.87	2.32	4.20	0.18	0.45	0.78
STM-FD00233 A010–22		1.04	0.23	0.39	0.33	2.00	2.10	4.10	0.16	0.49	0.70
STM-FD00233 A010–26		0.17	0.02	0.09	0.08	0.38	4.37	4.75	0.23	0.08	0.91
STM-FD00233 A010–29		0.52	0.17	0.33	0.17	1.20	3.61	4.80	0.14	0.25	0.90
STM-FD00233-A11		0.12	0.04	0.05	0.17	0.38	4.34	4.72	0.44	0.08	0.76
STM-FD00233-A12		0.37	0.05	0.32	0.00	0.73	12.33	13.06	0.00	0.06	1.95
STM-FD00233-A14	Batatal Formation - NE area	0.08	0.01	0.05	0.00	0.13	8.85	8.99	0.00	0.01	1.43
STM-FD00233-A16		0.10	0.01	0.06	0.00	0.17	7.30	7.48	0.00	0.02	1.02

* FeT and Al were calculated from the average of the following intervals. The total interval is 1.5 m.

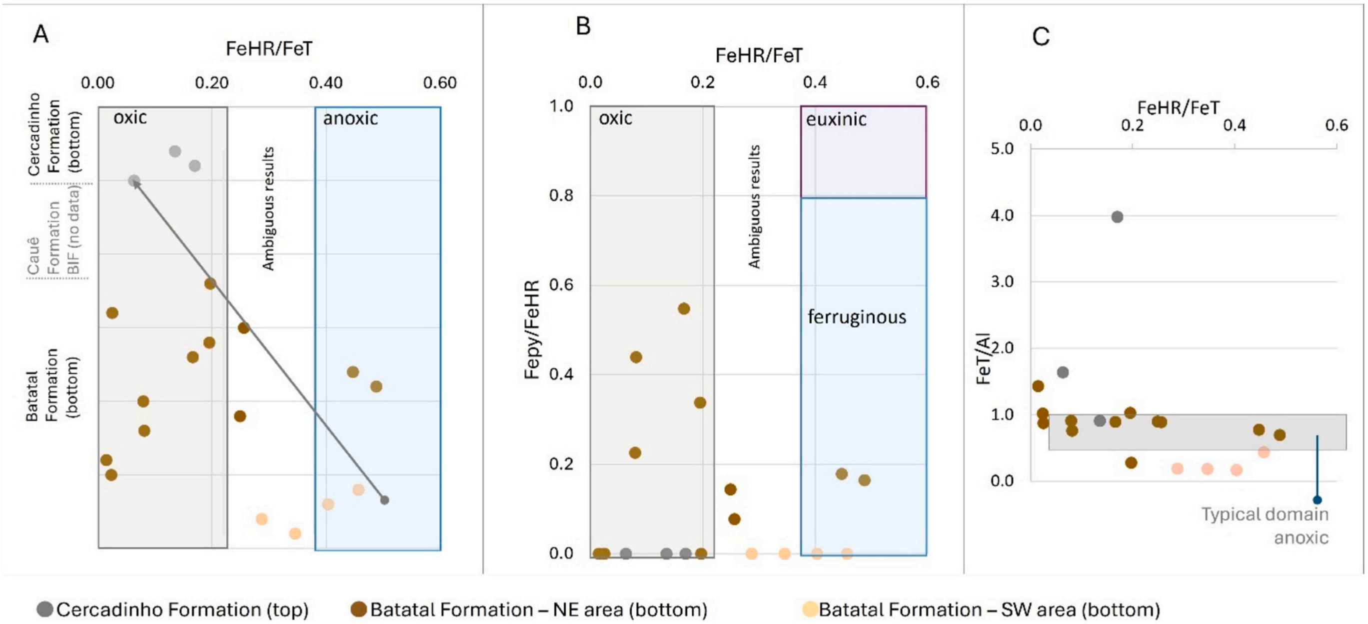

Fig. 7. (A) and (B) Iron speciation parameters used to evaluate ocean redox conditions based on metapelitic rock samples from the Batatal Formation (pre-Cauê BIF) and the Cercadinho Formation (post-Cauê BIF). (C) The FeT/Al and FeHR/FeT ratios serve as proxies for iron enrichment in the paleoenvironment. In this case, the inverse correlation between these parameters suggests that FeHR/FeT, which is sensitive to the conversion of FeU (poorly reactive iron) to FeHR (highly reactive iron), may be influenced by depositional processes. Fe/Al ratios between 0.5 and 1 are generally indicative of anoxic conditions. Abbreviations: FeHR = highly reactive iron; FeT = total iron; Fepy = pyritic iron.

0.22. In this area, the Fe_{Py}/Fe_{HR} ratio ranges from 0 to 0.55, with a median of 0.14. Notably, the protocol of Canfield et al. (1986) used here for Chromium Reducible Sulfur (i.e., Fe_{Py}) will also extract Acid Volatile Sulfur including pyrrhotite. Pyrrhotite can commonly form in metamorphic phases at the expense of pyrite or other highly reactive forms and cause erroneous interpretations (Slotznick et al., 2018). The general absence of Fe_{Py} as measured by chromium reduction indicates that conversion to pyrrhotite is not unduly affecting our interpretations.

In the uppermost stratigraphic succession, comprising the metasedimentary rocks from the Cercadinho Formation, the Fe_{HR}/Fe_{T} values are 0.06, 0.14 and 0.17 wt%, with a median of 0.12. Similar to the Batatal phyllite, the Fe_{Py}/Fe_{HR} ratio in this unit is also zero, indicating the absence of pyrite and/or pyrrhotite.

5. Discussion

5.1. Paleosalinity reconstruction

Paleosalinity proxies potentially record temporal changes in the water salinity, providing estimates of fresh, brackish, and marine conditions in ancient basins (Potter et al., 1963; Wei et al., 2018; Gilleaudeau et al., 2021; Remírez et al., 2024). As indicated by Wei and Algeo (2020), salinity levels are classified using multiple geochemical ratios, such as B/Ga, Sr/Ba and S/TOC, obtained from fine-grained sediments like shale or mudstone. These ratios represent the preferential concentration of certain elements under varying water salinities. For example, B and Sr exhibit conservative behaviour in saline water, while Ga and Ba are readily absorbed by clay minerals in freshwater sediments (Sirocko, 1995; Millero et al., 2008; Wei et al., 2018) and their abundance is usually related closely to the detrital and freshwater input (Wei and Algeo, 2020; Schier et al., 2021). The relative concentrations of buried S and TOC also differ between marine and non-marine sedimentary facies primarily because sulfate is present at extremely low concentrations in freshwaters as compared to marine waters (Berner, 1985).

Reference values from Wei and Algeo (2020) provide a guideline for interpreting paleosalinity proxies: (i) B/Ga <3 is freshwater; 3 to 6 is brackish; and > 6 is marine; (ii) Sr/Ba <0.2 is freshwater; 0.2 to 0.5 is brackish; and > 0.5 is marine; (iii) S/TOC <0.1 is freshwater, and > 0.1 indicates brackish or marine. Liu et al. (2025) Updated that Sr abundance in Proterozoic rocks is significantly lower than in modern seawater and suggested adjusting the Sr/Ba parameter for Proterozoic depositional systems, redefining freshwater (<0.08), brackish (0.08–0.20), and marine (>0.20) salinity facies

The analyzed samples from the Quadrilátero Ferrífero reveal a salinity gradient in the Batatal Formation, as indicated by the three paleosalinity proxies. Broadly, salinity increases from the southwestern to the northeastern areas, a pattern likely reflecting either greater freshwater input in the southwest or better connectivity to the open ocean in the northeast. Within the Cercadinho Formation, at the top of the stratigraphy, paleosalinity data confirms that these fine-grained sedimentary rocks were deposited in a marine environment. A detailed discussion of each paleosalinity proxy and its preservation is provided in the following section.

5.1.1. Potential effects of post-depositional alteration

Given that many of the elements used as paleosalinity proxies are initially adsorbed onto clay mineral, which recrystallize during metamorphic transformation into phyllite, there is a high likelihood of elemental mobility that could affect the proxies and their interpretive framework (which is based on modern sediments that have not even undergone diagenesis; Wei and Algeo, 2020). However, the crystalline structure and composition of clay minerals may play an important role in limiting the mobility of elements during diagenesis and low-grade metamorphism (Dohmeier et al., 1996; Liu et al., 2025). For example, several studies have discussed the potential preservation of paleosalinity proxies during burial and low-grade metamorphism (Środoń, 2010; Retallack, 2020; Cheng et al., 2021; Wang et al., 2021; Yu et al., 2022; Wei et al., 2024). Liu et al. (2025) reported no evidence of significant gain or loss of B, Ba, Ga, and Sr in clay minerals after burial diagenesis. This work demonstrated that paleosalinity ratios remained consistent despite variations in burial temperature, from 125 to 150 °C in metasiliciclastic rocks of the Nonesuch Formation (Michigan, USA) to 260–330 °C in the Datangpo Formation (Guizhou Province, China), suggesting that they can be preserved during diagenesis and metamorphic processes.

In the Quadrilátero Ferrífero, Paleoproterozoic rocks exhibit evidence for the preservation of geochemical and isotopic signals in metasedimentary rocks, as demonstrated through i) the consistent carbon isotopic signatures obtained in dolostones (Bekker et al., 2003; De Paula et al., 2023), ii) REE concentrations in BIFs (e.g. Spier et al., 2007; Alkmim, 2014; Teixeira et al., 2017) and iii) minimal deformation observed in the area, as evidenced by well-preserved primary structures (Madureira et al., 2021), stromatolites and oncolites (Souza and Müller, 1984; Babinski et al., 1995). In addition, fluid inclusion studies conducted in the eastern part of the province indicate that fluid-rock interactions in hematite from BIF layers recorded temperatures between 140 and 205 °C, suggesting minimal metamorphic alteration, while quartz grains reached higher temperatures of 280–351 °C (Rosière and Rios, 2004; Rosière et al., 2008).

Therefore, the integration of geochemical datasets with a well-constrained regional stratigraphic and sedimentological framework in the Quadrilátero Ferrífero (e.g., Madureira et al., 2021; Gonçalves and Uhlein, 2022) supports the interpretation and validates the application of these proxies, demonstrating that the signal shows consistency in a directional sense and is present across multiple proxies, which enhances confidence in the overall interpretation.

5.1.2. B—Ga proxy

Within the Batatal Formation, southwestern phyllites (GAD-SW) have lower B/Ga values (median 0.9), increasing toward the northeastern region (median 1.8). The southwestern phyllites exhibit a higher median Ga value of 36 ppm (range 27–39 ppm), while the northeast area shows a wider range of 24 ppm (15–51 ppm). These variations in Ga concentration may reflect more significant freshwater input from the southwestern than from the northeastern.

In the Cercadinho Formation, the upper stratigraphic unit, B/Ga values increase (median/range: 1.1 / 0.7–5.6), among which, two out of five samples acquire B/Ga of 4.5 and 5.6, indicating close to fully marine conditions as defined by Wei and Algeo (2020). This trend aligns with the slight decrease in Ga concentrations (median: 31 ppm; range: 4–37 ppm), indicating increasing salinity levels. The similarity in B/Ga ratios between the Cercadinho Formation and modern sediments suggests that Paleoproterozoic seawater salinity may have been comparable to that of the modern ocean, consistent with the parameters proposed by Knauth (2005), who argued that the most significant decline in ocean salinity occurred during the Neoproterozoic, coinciding with the formation of the first known large salt deposits. However, the observed secular variations in water mass correspond closely with the depositional evolution of the Minas Basin, reflecting dynamic changes in paleoenvironmental conditions during its formation. Therefore, the B/Ga values indicate a transition from freshwater-brackish facies in the Batatal Formation to fully marine conditions in the Cercadinho Formation from the bottom up (Figs. 6 and 8).

5.1.3. Sr—Ba proxy

The Sr/Ba data show an upward trend in younger rocks, ranging from 0.04 to 0.62 (Fig. 8). In the southwestern Batatal phyllites (GAD-SW), Sr/Ba values are low (median 0.09, range 0.08–0.11), while northeastern samples show more variability (median 0.17, range 0.04–0.46), indicating freshwater to brackish conditions. These paleosalinity results are consistent with the rock assemblages found in each specific area. In GAD-SW, homogeneous sericitic phyllites dominate,

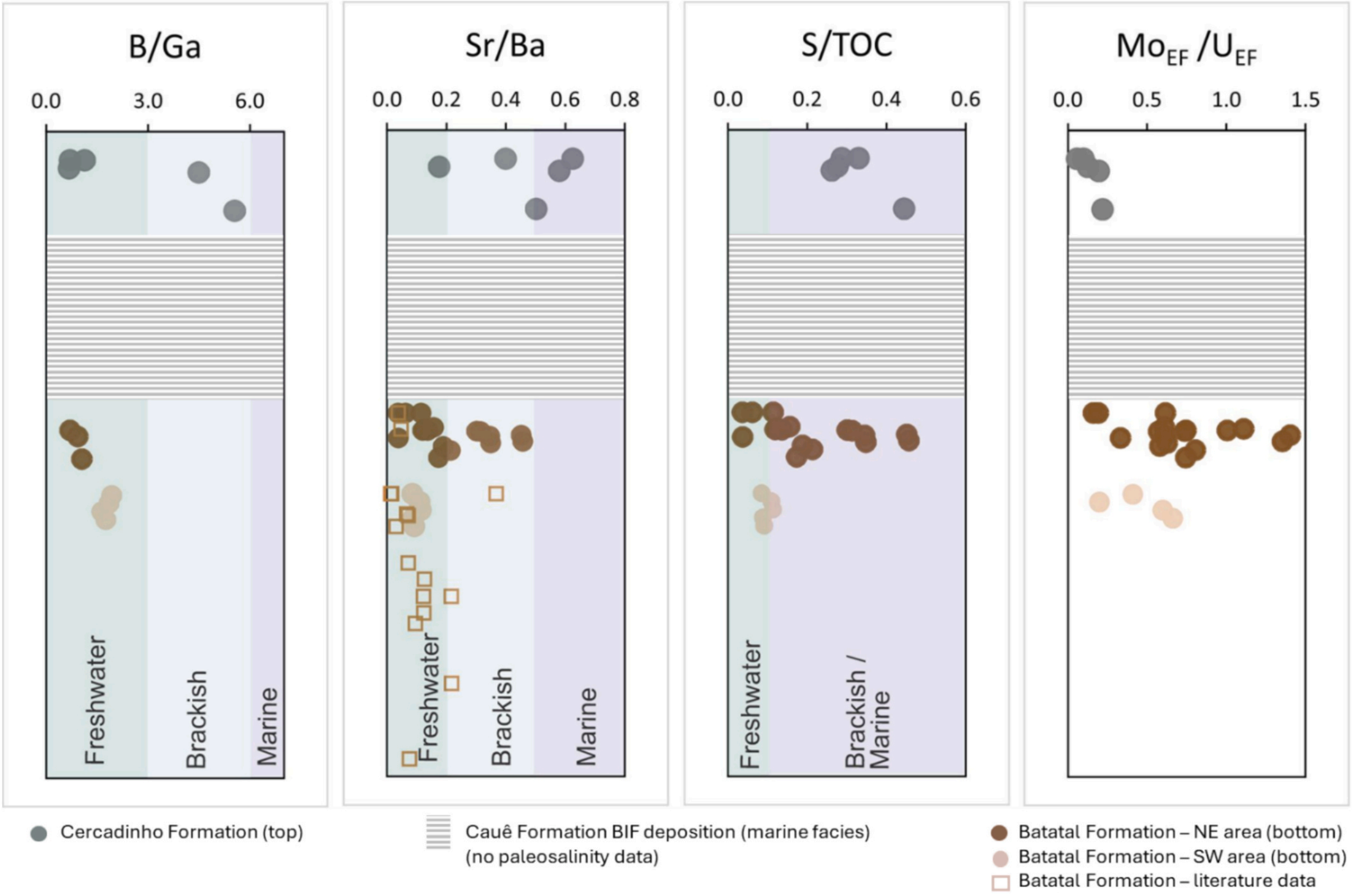

Fig. 8. Profile of B/Ga, Sr/Ba, S/TOC, and Mo_{EF}/U_{EF} represents the modern reference values for paleosalinity reconstruction applied to studied metamorphic fine-grained sedimentary rocks. The horizontal datum (base contact of the Cauê and Batatal formations) was used to calculate the relative depth (see Fig. 3).

whereas GAD-NE represents a transitional environment with contributions from chemical sedimentary rocks. Other studies (Spier et al., 2007; Alkmim, 2014; Hensler et al., 2017) report similarly low Sr/Ba values in Batatal phyllites, supporting the interpretation of a predominantly freshwater environment during their deposition (Fig. 8). Interestingly, these reference data, which indicate low Sr/Ba ratios characteristic of freshwater facies (Fig. 8), come from locations only 30 km away from the study area of this work (Fig. 1).

In the Cercadinho Formation, Sr/Ba values rise to a median of 0.50 (range 0.40–0.62), with one outlier (0.17). These values suggest marine facies sedimentation during a transgressive phase following the deposition of the Cauê BIF and Gandarela carbonates (Dorr, 1969; Gonçalves and Uhlein, 2022).

Overall, the Sr/Ba proxy reveals a transition in the paleosalinity conditions. Initially, the sediments at the base of the stratigraphy reflect freshwater to low brackish conditions suggesting a weak circulation with the open ocean, and transgression shifted the environment to marine deposition within the Itabira and Piracicaba Groups (Fig. 8).

5.1.4. S-TOC proxy

Sulfur and TOC concentrations are key indicators of paleosalinity, as S is more abundant in marine sediments due to microbial sulfate reduction and pyrite formation (Gilleaudeau et al., 2021). On the other hand, the abundance of TOC in the sedimentary rocks is associated with large microbial populations, sedimentation rates, and biomass preservation in estuarine, deltaic or coastal settings (Berner, 1985; Playter et al., 2017). The S/TOC ratio is about 13 times higher in marine than in freshwater sediments, making it a reliable paleosalinity proxy (Wei and Algeo, 2020).

The S-TOC results align with other proxies (e.g. Sr/Ba ratio and B/Ga ratios), showing increasing salinity toward the Cercadinho Formation (Figs. 6 and 8). In contrast, the Cercadinho Formation's S/TOC values indicate fully marine facies, reinforcing a marine transgressive scenario.

It is possible that the results of TOC in the present day doesn't represent for the original content, as part of the organic matter may have migrated out of the rock during burial and thermal maturation (Hart and Hofmann, 2022; Olson et al., 2025). Similarly, S abundance may have been affected by mobilization from the rocks (Hart and Hofmann, 2022). Reconstructing the original TOC content using Jarvie (2012) method is challenging in this study due to the low TOC abundance. Despite the uncertainties related to post-depositional alterations in the studied samples, the S/TOC results remain consistent with other paleosalinity proxies and align with the evolution of the Minas Basin.

In summary, these paleosalinity proxies (B/Ga, Sr/Ba, and S/TOC) indicate a transition from freshwater to low-brackish conditions in the Batatal Formation to fully marine conditions in the Cercadinho Formation.

5.2. Paleoredox variation in the Minas Basin

Iron speciation results indicate a wide range of values associated with ferruginous to oxic conditions, with Fe_{HR}/Fe_T values ranging from 0.49 to 0.06, peaking in the Batatal formation (Fig. 7A). The inverse relationship between Fe_{HR}/Fe_T and Fe_T/Al (Fig. 7C and D) suggests that the Fe_{HR}/Fe_T ratio, which is sensitive to the conversion of Fe_U to Fe_{HR}, may be influenced by post-depositional processes. For example, some highly reactive (HR) iron pools may have been converted to silicates or carbonates during metamorphism, thereby transferring it to the Fe_U pool and causing the Fe_{HR}/Fe_T ratio to drop below 0.2 in some samples (Slotznick et al., 2018; Raiswell et al., 2018). Furthermore, samples that were deposited rapidly may not exhibit the authigenic enrichments that the iron speciation proxy attempts to fingerprint, yielding spuriously low Fe_{HR}/Fe_T. Thus, considering the factors mentioned above, samples with $Fe_{HR}/Fe_T > 0.38$ are interpreted as deposited under anoxic bottom water conditions, while lower values suggest oxic conditions (Poulton and Canfield, 2011; Caxito et al., 2024). However, due to the discrepancy between Fe_T/Al and Fe_{HR}/Fe_T ratios (Fig. 7C), the iron speciation data cannot be directly taken at face value to confirm oxic bottom water conditions.

The low Fe_{Py}/Fe_{HR} ratio ($<$0.55 wt%) indicates an overall absence of euxinic conditions (Fig. 7B). In contrast, the high Fe_T/Al and high Fe_{HR}/Fe_T ratios strongly suggest anoxic bottom water conditions. It is important to note that the iron speciation proxy reflects redox conditions at the sediment/water interface (i.e., bottom water conditions) rather than in surface waters (Poulton and Canfield, 2011; Raiswell et al., 2018). This means that the Minas Basin was probably stratified, with a shallow oxic layer where dissolved ferrous iron (FeII) was oxidized and precipitated, overlying ferruginous bottom waters where the iron accumulated. This stratification aligns with existing models for BIF deposition in the Minas Basin (Teixeira et al., 2017). Our study also highlights the challenges in applying iron-speciation redox proxies to ancient basins, particularly in iron-rich intervals and basins that have experienced substantial metamorphism.

The EF values of the RSE in phyllite samples (Fig. 6) indicate significant enrichment in the Batatal phyllites at the base of the stratigraphy, with maximum values of Cr_{EF} (3), V_{EF} (3.9), U_{EF} (6.7), and Mo_{EF} (6.3). Notably, the Batatal carbonaceous phyllite in the NE area exhibits a pronounced increase in RSEs (Fig. 6). Additionally, the distribution of Mo_{EF}/U_{EF} values, as outlined by Algeo and Tribovillard (2009), serves as another redox proxy. This proxy is valuable for identifying reducing conditions, as Mo is preferentially scavenged in euxinic (oxygen-depleted, sulfur-rich) environments, while U is more likely to be scavenged in anoxic settings more broadly (irrespective of sulfide levels) (Algeo and Maynard, 2008; Tostevin and Mills, 2020). This differentiation provides critical insight into the predominantly suboxic redox conditions during deposition of the Batatal and Cercadinho formations (Figs. 6, 9). The EF values of RSE (e.g. Mo, U, Cu and Ni), along with Mo_{EF}/U_{EF}, indicate generally suboxic-anoxic conditions during the Batatal Formation deposition. In contrast, the Cercadinho Formation seems to exhibit more distinctly suboxic conditions, likely reflecting increased O_2 levels in surface waters while maintaining persistent anoxic conditions at the seafloor.

The C_{org}/P ratio serves as a proxy for tracking redox changes in the Minas Basin, as low O_2 levels promote the preservation of organic carbon and P release, whereas oxygenated conditions lead to organic carbon degradation and P retention (Algeo and Ingall, 2007). According to thresholds proposed by Ingall and Van Cappellen (1990) and Remírez et al. (2024), a $C_{org}/P < 50$ indicates oxic-suboxic conditions. Samples

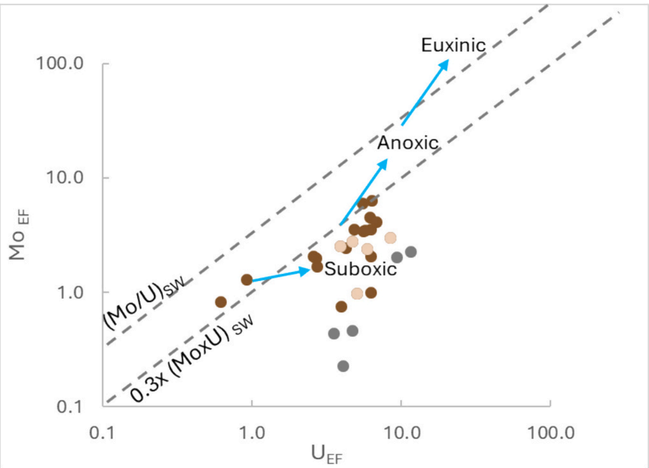

Fig. 9. Variation of enrichment of U and Mo in the Minas Basin (Algeo and Tribovillard, 2009). The gray circles represent the Cercadinho Formation, the dark brown, Batatal Formation – area NE and light brown, the Batatal Formation – area SW. (For interpretation of the references to colour in this figure legend, the reader is referred to the web version of this article.)

from the Batatal Formation, located at the base of the stratigraphy, exhibit a wider range of C_{org}/P values, with a median of 14.4 (0.8–97.6). This suggests lower O_2 levels compared to the Cercadinho Formation, which exhibits a lower median C_{org}/P value of 1.3 (0.7–6.7). These findings are consistent with the interpretation that Batatal Formation represents more reduced conditions than of the Cercadinho Formation.

The reconstruction of water mass conditions based on the correlation between redox and paleosalinity proxies has been previously demonstrated by Falkner et al. (1993), Remírez et al. (2024) and Wei et al. (2024). The relationship between the B/Ga ratio versus U_{EF} suggests dynamic water column conditions (Fig. 10) and a close correlation between salinity and redox condition. An integrated analysis of paleoredox proxies and paleosalinity proxies reveals the evolution of the water mass condition in the Minas Basin. Initially, during a suboxic-anoxic phase, limited connection to the open ocean resulted in a strongly stratified water column with oxygen-depleted deep waters. However, during the deposition of Cercadinho Formation, the basin became better connected to the open ocean, achieving fully marine salinity. Improved water circulation and ventilation led to increased O_2 levels in the water column.

5.3. *Evidence for bioproductivity in the Batatal phyllite*

The Batatal phyllite exhibits enrichment of Cu, Ni and Zn, particularly in the carbonaceous phyllite layers in the northeastern area. This elemental enrichment, along with the sedimentary record, serves as evidence of significant microbial phytoplankton activity in the surface water of the Minas paleobasin, as these trace elements are essential for bacterial cellular functions (e.g. Tribovillard et al., 2006; Scott et al., 2013; Han et al., 2021). Moreover, sedimentary records suggest the paleoenvironmental conditions were reducing, allowing for the accumulation and degradation of biomass. This process, combined with burial fluxes, contributed to the trace element enrichment observed in the sediments (Tribovillard et al., 2006; Algeo and Maynard, 2008; Playter et al., 2017).

Phosphorus is another essential element for life, yet it is not a reliable indicator of paleoproductivity because it can be extensively recycled within the water column under anoxic conditions (Tribovillard et al., 2006). Nevertheless, Algeo and Ingall (2007) discuss variations in the C_{org}/P ratio as a proxy reflecting benthic redox conditions in depositional systems. Accordingly, the elevated C_{org}/P ratio values (97.9) found in the carbonaceous phyllites of the Batatal Formation suggest anoxic benthic redox conditions during their deposition.

This, coupled with other evidence, indicates elevated bioproductivity in the Minas Basin prior to the GOE and the precipitation of the Cauê BIF. This interpretation is consistent with the presence of free O_2 in the photic zone, which would have supported phytoplankton growth by providing essential nutrients derived from chemical weathering of terrestrial rocks (Hsi and Langmuir, 1985; Konhauser et al., 2011; Teixeira et al., 2017; Scott et al., 2008; Tostevin and Mills, 2020). The observed decrease of Cu, Ni and Zn abundance in the younger rocks from the Cercadinho Formation likely indicates a transition period where the paleoenvironmental changes impacted the biogeochemical cycling of trace elements.

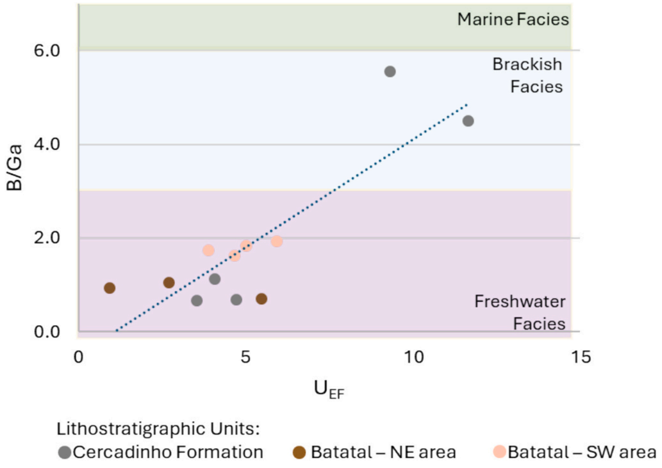

Fig. 10. Correlation between paleosalinity and redox proxies.

5.4. *Depositional model*

The Caraça Group outlines a record of the tectonic evolution of the Minas Basin, transitioning from a continental rift to a passive margin setting (Dorr, 1969). This sequence reflects a shift from continental sedimentation (Gonçalves and Uhlein, 2022; Madureira et al., 2021) to deposition on an extensive continental shelf (Dorr, 1969). In this context, the alluvial-fluvial deposits of the Moeda Formation are conformably overlain by fine-grained siliciclastic rocks of the Batatal Formation (Dorr, 1969; Gonçalves and Uhlein, 2022).

Our findings suggest that the Batatal Formation comprises both detrital and chemical rocks deposited in freshwater to slightly brackish environments (Fig. 11A and B). Fluvial influx transported continental sediments into a large freshwater body, interpreted as a lacustrine system, owing to the mixed siliciclastic-dolomitic deposition. Comparable examples can be found in other Brazilian sedimentary basins, such as the Cretaceous-aged Campos and Santos Basins, which both record the tectonic evolution from rift to post rift stage (e.g. Strugale and Cartwright, 2022). This progression is characterized by the initial deposition of fine-grained sediments in continental lacustrine environments, followed by a transition to marine sedimentation on shallow to deep marine platforms (Moreira et al., 2007; Winter et al., 2007).

In the studied profile, the Batatal phyllite records a salinity gradient increase from the southwest to the northeast, based on the current orientation of the sedimentary layers in the Gandarela Syncline (Fig. 2A). This observation suggests that, in the northeastern portion, the freshwater body may have a partial connection with the ocean, leading to water mixing and the development of brackish conditions (Fig. 11B). During this stage of the sedimentary basin's evolution, the water column likely exhibited suboxic conditions within a stratified basin, characterized by a (sub)oxygenated surface layer overlying anoxic bottom water. Subsequently, as the transgressive system advanced, deposition transitioned to a fully marine environment, marked by the deposition of BIF (Cauê Formation) and carbonates (Gandarela Formation). At the top of the stratigraphic sequence, the Cercadinho Formation reflects sedimentation in a marine environment under less-reducing conditions, indicative of improved ventilation and oxygenation in the basin (Fig. 11C).

Therefore, the Minas Basin provided localized conditions conducive to the deposition of Fe-mineral precursors of BIF, prior to the Cauê BIF, in a transitional paleoenvironment influenced by a mix of waters with varying salinities, as evidenced by the Batatal Formation. In contrast, the formation of the giant iron deposits in the Quadrilátero Ferrífero, represented by the Cauê BIF (~350 m thick), followed by the Gandarela dolostones (~350 m thick), reflects a period of stable water mass conditions. These conditions facilitated the accumulation of these massive iron deposits over a timespan of approximately 100 million years.

6. Conclusion

Comprehensive paleosalinity studies using multiple salinity proxies (B/Ga, Sr/Ba and S/TOC ratios) reveal dynamic changes in water mass conditions throughout the formation of the Minas Basin. The fine-grained sediments of the Batatal Formation, located at the base of the stratigraphy, record a transition from freshwater to low-brackish facies, with limited marine influence. This suggests that the depositional paleoenvironment of the Batatal Formation was dominated by continental sedimentation. As a marine transgression advanced, the

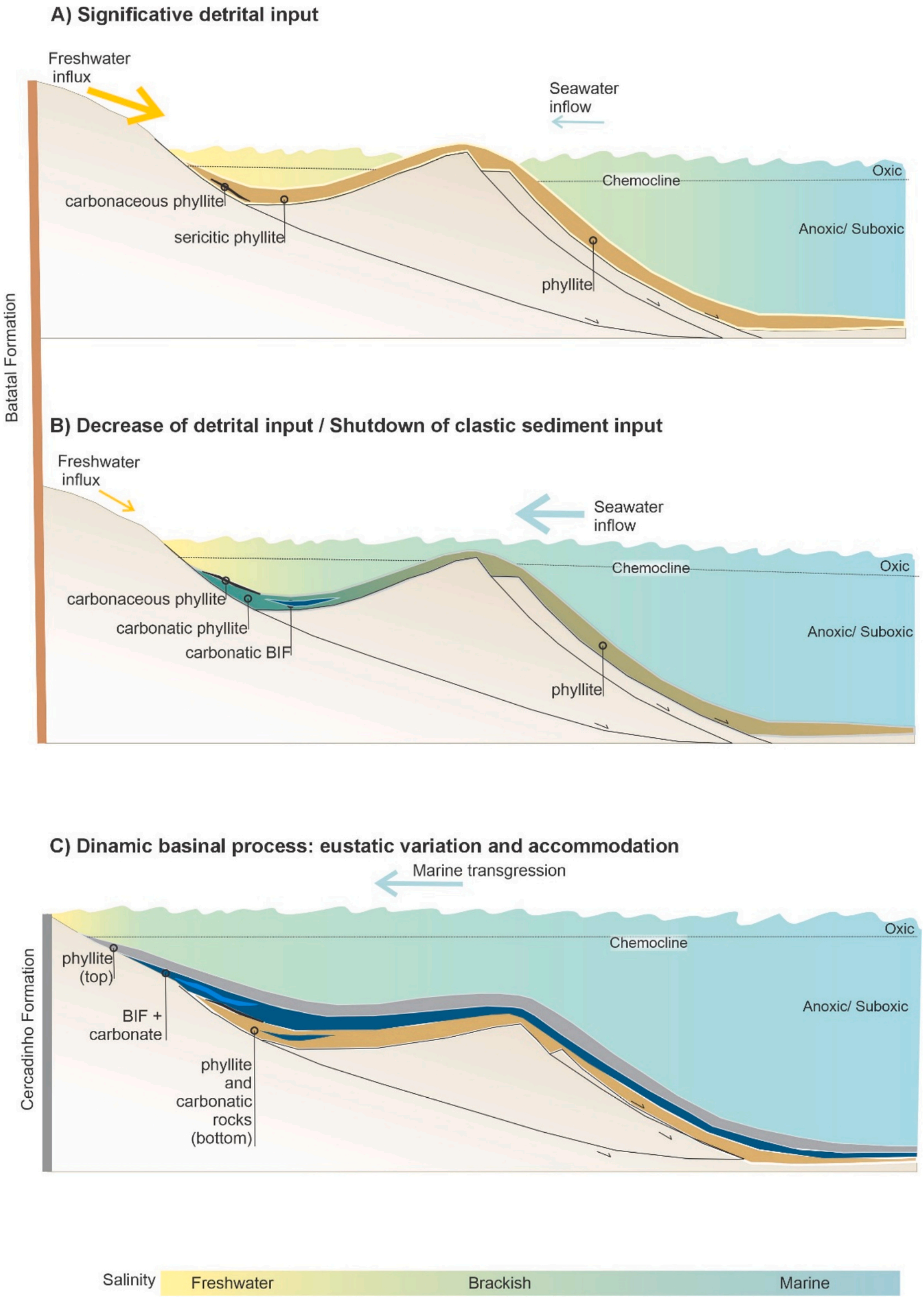

Fig. 11. Schematic depositional model for the Minas succession. (A and B) older Batatal Formation, highlighting variations in sediment input types and changes in base level. (C) Representation of the younger Cercadinho Formation showing detrital sedimentation during a later evolutionary stage of the Minas Basin.

depositional environment shifted toward fully marine conditions, coinciding with the deposition of the Cauê BIF, Gandarela carbonates, and fine-grained sediments of the Cercadinho Formation. Therefore, the onset of BIF deposition is linked to a transitional paleoenvironment subject to mixed-salinity waters (Batatal Formation), while the giant iron deposits of the Quadrilátero Ferrífero, including the Cauê BIF, likely formed under stable water mass conditions sustained for ~100 million years.

This study indicates that paleosalinity proxies (B/Ga, Sr/Ba, and S/TOC) can provide reliable results even in metamorphic rocks, serving as valuable tools for reconstructing depositional environments. It underscores their potential for investigating Paleoproterozoic rocks while also highlighting the need for further research on how these proxies behave during metamorphism.

Paleoredox reconstructions suggest that the Batatal phyllites were deposited under anoxic and ferruginous (non-euxinic) bottom-water conditions. On the other hand, the younger Cercadinho Formation phyllites, found at the top of the stratigraphy, exhibit depleted RSE abundances, and lower Fe_{HR}/Fe_T ratios, but high Fe/Al ratios suggest iron re-partitioning due to post-depositional processes. Further investigation is needed to determine whether the fine-grained sediments of the Cercadinho Formation reflect less-reducing waters, with enhanced water column ventilation leading to improved deep-water oxygenation.

CRediT authorship contribution statement

Janaina Rodrigues de Paula: Writing – review & editing, Writing – original draft, Visualization, Validation, Software, Project administration, Investigation, Formal analysis, Data curation, Conceptualization. **Wei Wei:** Writing – review & editing, Writing – original draft, Validation, Methodology, Investigation, Formal analysis, Data curation, Conceptualization. **Fabricio A. Caxito:** review & editing, Conceptualization. **Katherine N. Snihur:** Writing – review & editing, Formal analysis. **Cody N. Lazowski:** Writing – review & editing, Formal analysis. **Kurt O. Konhauser:** Writing – review & editing, Supervision, Resources, Investigation, Funding acquisition, Conceptualization. **Erik A. Sperling:** Writing – review & editing, Resources, Methodology. **Daniel S. Alessi:** Resources, Funding acquisition.

Declaration of competing interest

All authors: Janaina Rodrigues de Paula, Wei Wei, Fabricio A. Caxito, Katherine N. Snihur, Cody N. Lazowski, Kurt O. Konhauser, Erik A. Sperling, Daniel. Alessi confirm that there are no known conflicts of interest associated with this publication and there has been no significant financial support for this work that could have influenced its outcome.

Acknowledgments

The authors would like to thank the mining company VALE S.A. for its collaboration and financial support, especially through ADIMB collaborative project: VALE - UNIVERSITIES - INSTITUTIONS (Brazil). JRP was supported by CAPES, FAPEMIG, and Instituto Serrapilheira scholarships (Brazil) FAC is a recipient of a Research Productivity Grant from the Conselho Nacional de Pesquisa Científica (CNPq) and acknowledge for the support received through grants nb. 408815/2021-3 and 304509/2021-3. This is a contribution to Project MOBILE (geolifemobile.com), supported by Instituto Serrapilheira, Brazil (grant nb Serra-1912-31510). KOK was funded by the Natural Sciences and Engineering Research Council of Canada (NSERC). EAS was funded by a National Science Foundation grant EAR-2143164. The project was supported by the "CUG Scholar" Scientific Research Funds at China University of Geosciences (Wuhan) (Project No. 2022153).

Data availability

All the data utilized in this study are presented in the paper as tables.

References

Alcott, L.J., Krause, A.J., Hammarlund, E.U., Bjerrum, C.J., Scholz, F., Xiong, Y., Poulton, S.W., 2020. Development of iron speciation reference materials for palaeoredox analysis. Geostand. Geoanal. Res. 44 (3), 581–591. https://doi.org/10.1111/ggr.12342.

Algeo, T.J., Ingall, E., 2007. Sedimentary Corg: P ratios, paleocean ventilation, and Phanerozoic atmospheric pO2. Palaeogeogr. Palaeoclimatol. Palaeoecol. 256 (3–4), 130–155. https://doi.org/10.1016/j.palaeo.2007.02.029.

Algeo, T.J., Maynard, J.B., 2008. Trace-metal covariation as a guide to water-mass conditions in ancient anoxic marine environments. Geosphere 4 (5), 872–887. https://doi.org/10.1130/GES00174.1.

Algeo, T.J., Tribovillard, N., 2009. Environmental analysis of paleoceanographic systems based on molybdenum–uranium covariation. Chem. Geol. 268 (3–4), 211–225. https://doi.org/10.1016/j.chemgeo.2009.09.001.

Alkmim, A.R., 2014. Investigação geoquímica e estratigráfica da Formação Ferrífera Cauê na porção centro—oriental do Quadrilátero Ferrífero. MG. Dissertation on Graduate Departament in Geology. Escola de Minas, Universidade de Ouro Preto, Ouro Preto, p. 178.

Alkmim, F., Marshak, S., 1998. Transamazonian orogeny in the Southern Sao Francisco craton region, Minas Gerais, Brazil: evidence for Paleoproterozoic collision and collapse in the Quadrilátero Ferrífero. Precambrian Res. 90 (1), 29–58. https://doi.org/10.1016/S0301-9268(98)00032-1.

Babinski, M., Chemale Jr., F., Van Schmus, W., 1995. The Pb/Pb age of the Minas Supergroup carbonate rocks, Quadrilátero Ferrífero, Brazil. Precambrian Res. 72 (3–4), 235–245. https://doi.org/10.1016/0301-9268(94)00091-5.

Bekker, A., Sial, A.N., Karhu, J.A., Ferreira, V.P., Noce, C.M., Kaufman, A.J., Pimentel, M. M., 2003. Chemostratigraphy of carbonates from the Minas Supergroup, Quadrilátero Ferryífero (Iron Quadrangle), Brazil: a stratigraphic record of early Proterozoic atmospheric, biogeochemical and climactic change. Am. J. Sci. 303 (10), 865–904. https://doi.org/10.2475/ajs.303.10.865.

Berner, R.A., 1985. Sulphate reduction, organic matter decomposition and pyrite formation. Philos. Trans. R. Soci. London Series A Math. Phys. Sci. 315 (1531), 25–38. https://doi.org/10.1098/rsta.1985.0027.

Brand, U., Veizer, J., 1980. Chemical diagenesis of a multicomponent carbonate system; 1, Trace elements. J. Sediment. Res. 50 (4), 1219–1236. https://doi.org/10.1306/212F7BB7-2B24-11D7-8648000102C1865D.

Cabral, A.R., Zeh, A., Koglin, N., Gomes Jr., A.A.S., Viana, D.J., Lehmann, B., 2012. Dating the Itabira iron formation, Quadrilátero Ferrífero of Minas Gerais, Brazil, at 2.65 Ga: depositional U–Pb age of zircon from a metavolcanic layer. Precambrian Res. 204, 40–45. https://doi.org/10.1016/j.precamres.2012.02.006.

Canfield, D.E., Raiswell, R., Westrich, J.T., Reaves, C.M., Berner, R.A., 1986. The use of chromium reduction in the analysis of reduced inorganic sulfur in sediments and shales. Chem. Geol. 54 (1–2), 149–155. https://doi.org/10.1016/0009-2541(86)90078-1.

Canuto, J.R., 2010. Estratigrafia de sequências em bacias sedimentares de diferentes idades e estilos tectônicos. Rev. Bras. Geoci. 40 (4), 537–549.

Caxito, F.A., Sperling, E., Fazio, G., Adorno, R.R., Denezine, M., Do Carmo, D.A., Sial, A. N., 2024. A shift in redox conditions near the Ediacaran/Cambrian transition and its possible influence on early animal evolution, Corumbá Group, Brazil. Geosci. Front. 15 (4), 101810. https://doi.org/10.1016/j.gsf.2024.101810.

Chemale Jr., F., Rosiere, C.A., Endo, I., 1994. The tectonic evolution of the Quadrilátero Ferrífero, Minas Gerais, Brazil. Precambrian Res. 65 (1–4), 25–54. https://doi.org/10.1016/0301-9268(94)90098-1.

Cheng, M., Zhang, Z., Algeo, T.J., Liu, S., Liu, X., Wang, H., Li, C., 2021. Hydrological controls on marine chemistry in the Cryogenian Nanhua Basin (South China). Earth Sci. Rev. 218, 103678. https://doi.org/10.1016/j.earscirev.2021.103678.

Daher, A.P., Costa, M.A., Novo, T.A., 2020. A Serra das Cambotas: terminação Meridional do Supergrupo Espinhaço no Quadrilátero Ferrífero. MG. Geonomos 28 (1), 15–24. https://doi.org/10.18285/geonomos.v28i1.29651.

De Paula, J.R., Caxito, F.A., Sial, A.N., Ribeiro, D.T., Alkmim, A.R., Lana, C., Endo, I., 2023. Trace elements, C–O isotopes and U–Pb geochronology of the Minas Supergroup in the Segredo deposit, Quadrilátero Ferrífero, Brazil. J. S. Am. Earth Sci. 129, 104525. https://doi.org/10.1016/j.jsames.2023.104525.

Dohmeier, C., Loos, D., Schnöckel, H., 1996. Aluminum (I) and gallium (I) compounds: syntheses, structures, and reactions. Angewandte Chemie International Edition in English 35 (2), 129–149.

Dopico, C.I.M., Lana, C., Moreira, H.S., Cassino, L.F., Alkmim, F.F., 2017. U–Pb ages and Hf-isotope data of detrital zircons from the late Neoarchean-Paleoproterozoic Minas Basin, SE Brazil. Precambrian Res. 291, 143–161. https://doi.org/10.1016/j.precamres.2017.01.026.

Dorr, J.V.N., 1969. Physiographic, Stratigraphic, and Structural Development of the Quadrilátero Ferrífero, Minas Gerais, Brazil. US Gov. Print. Office, 641-A. 118p.

Dutra, L.F., Dias, S.P., Martins, M., Lana, C., Batista, A.C., Tavares, T.D., 2020. Detrital zircon records of the Paleo-Mesoproterozoic rift-sag Tamanduá Group in its type-section, Northern Quadrilátero Ferrífero, Minas Gerais, Brazil. Brazili. J. Geol. 50, e20190069. https://doi.org/10.1590/2317-4889202020190069.

Endo, I., Galbiatti, H.F., Delgado, C.E.R., de Oliveira, M.M.F., de Zapparoli, A.C., de Moura, L.G.B., Carlos, D.U., 2019. Mapa geológico do Quadrilátero Ferrífero, Minas Gerais, Brasil. Escala 1:150.000. Departamento de Geologia, Escola de Minas – UFOP - Centro de Estudos Avançados do Quadrilátero Ferrífero, Ouro Preto.

Endo, I., Machado, R., Galbiatti, H.F., Rossi, D.Q., de Zapparoli, A.C., Delgado, C.E.R., Oliveira, M.M.F., 2020. Estratigrafia e evolução estrutural do Quadrilátero Ferrífero, Minas Gerais. In: Castro, P.T.A., Endo, I., Gandini, A.L. (Eds.), Quadrilátero Ferrífero: Avanços do conhecimento nos últimos 50 anos, Belo Horizonte, pp. 70–113.

Falkner, K.K., Bowers, T.S., Todd, J.F., Lewis, B.L., Landing, W.M., Edmond, J.M., 1993. The behavior of barium in anoxic marine waters. Geochim. Cosmochim. Acta 57 (3), 537–554. https://doi.org/10.1016/0016-7037(93)90366-5.

Farina, F., Albert, C., Dopico, C., Moreira, H., Hippertt, J., Lana, C., 2016. The Archean–Paleoproterozoic evolution of the Quadrilátero Ferrífero (Brasil): Current models and open questions. J. S. Am. Earth Sci. 68, 4–21. https://doi.org/10.1016/j.jsames.2015.10.015.

Gilleaudeau, G.J., Algeo, T.J., Lyons, T.W., Bates, S., Anbar, A.D., 2021. Novel watermass reconstruction in the early Mississippian Appalachian Seaway based on integrated proxy records of redox and salinity. Earth Planet. Sci. Lett. 558, 116746. https://doi.org/10.1016/j.epsl.2021.116746.

Gonçalves, G.F., Uhlein, A., 2022. Depositional systems, sequence stratigraphy, and sedimentary provenance of the Palaeoproterozoic Minas Supergroup and Itacolomi Group, Quadrilátero Ferrífero, Brazil. Brazili. J. Geol. 52. https://doi.org/10.1590/2317-4889202220210081.

Gonçalves-Dias, T.G., de Silva, R.C.F., Lobato, L.M., de Andrade Caxito, F., Hagemann, S., Santos, J.O.S., Barrote, V., 2022. Ediacaran-Cambrian fluid flow in Archean orogenic gold deposits: Evidence from U–Pb SHRIMP hydrothermal monazite ages of the metaturbidite-hosted Córrego do Sítio and Pilar deposits, Quadrilátero Ferrífero, Brazil. J. S. Am. Earth Sci. 116, 103844. https://doi.org/10.1016/j.jsames.2022.103844.

Hagemann, S.G., Angerer, T., Duuring, P., Rosière, C.A., de Silva, R.F., Lobato, L., Walde, D.H.G., 2016. BIF-hosted iron mineral system: a review. Ore Geol. Rev. 76, 317–359. https://doi.org/10.1016/j.oregeorev.2015.11.004.

Han, X., Tomaszewski, E.J., Schoenberg, R., Konhauser, K.O., Amor, M., Pan, Y., Byrne, J.M., 2021. Using Zn and Ni behavior during magnetite precipitation in banded iron formations to determine its biological or abiotic origin. Earth Planet. Sci. Lett. 568, 117052. https://doi.org/10.1016/j.epsl.2021.117052.

Hart, B.S., Hofmann, M.H., 2022. Revisiting paleoenvironmental analyses and interpretations of organic-rich deposits: the importance of TOC corrections. Org. Geochem. 170, 104434. https://doi.org/10.1016/j.orggeochem.2022.104434.

Hartmann, L.A., Endo, I., Suita, M.T.F., Santos, J.O.S., Frantz, J.C., Carneiro, M.A., McNaughton, N.J., Barley, M.E., 2006. Provenance and age delimitation of Quadrilátero Ferrífero sandstones based on zircon U–Pb isotopes. J. S. Am. Earth Sci. 20 (4), 273–285. https://doi.org/10.1016/j.jsames.2005.07.015.

Hensler, A.S., Rosière, C.A., Hagemann, S.G., 2017. Iron oxide mineralization at the contact zone between phyllite and itabirite of the Pau Branco deposit, Quadrilátero Ferrífero, Brazil—implications for fluid-rock interaction during iron ore formation. Econ. Geol. 112 (4), 941–982. https://doi.org/10.2113/econgeo.112.4.941.

Hsi, C.K.D., Langmuir, D., 1985. Adsorption of uranyl onto ferric oxyhydroxides: application of the surface complexation site-binding model. Geochim. Cosmochim. Acta 49 (9), 1931–1941. https://doi.org/10.1016/0016-7037(85)90088-2.

Ingall, E.D., Van Cappellen, P., 1990. Relation between sedimentation rate and burial of organic phosphorus and organic carbon in marine sediments. Geochim. Cosmochim. Acta 54 (2), 373–386. https://doi.org/10.1016/0016-7037(90)90326-G.

Jarvie, D., 2012. Shale Resource Systems for Oil and Gas— Giant Resources for the 21st Century. AAPG Mem. 97, 1–19. https://doi.org/10.1306/13321446M973489.

Klein, C., Ladeira, E.A., 2000. Geochemistry and petrology of some Proterozoic banded iron-formations of the Quadrilátero Ferrífero, Minas Gerais, Brazil. Econ. Geol. 95 (2), 405–427. https://doi.org/10.2113/gsecongeo.95.2.405.

Knauth, L.P., 2005. Temperature and salinity history of the Precambrian Ocean: Implications for the course of microbial evolution. In: Geobiology: Objectives, Concepts, Perspectives. Elsevier, pp. 53–69. https://doi.org/10.1016/B978-0-444-52019-7.50007-3.

Koglin, N., Zeh, A., Cabral, A.R., Gomes Jr., A.A.S., Neto, A.V.C., Brunetto, W.J., Galbiatti, H., 2014. Depositional age and sediment source of the auriferous Moeda Formation, Quadrilátero Ferrífero of Minas Gerais, Brazil: New constraints from U–Pb–Hf isotopes in zircon and xenotime. Precambrian Res. 255, 96–108. https://doi.org/10.1016/j.precamres.2014.09.010.

Konhauser, K.O., Kappler, A., Roden, E.E., 2011. Iron in microbial metabolisms. Elements 7 (2), 89–93. https://doi.org/10.2113/gselements.7.2.89.

Konhauser, K.O., Planavsky, N.J., Hardisty, D.S., Robbins, L.J., Warchola, T.J., Haugaard, R., Johnson, C.M., 2017. Iron formations: a global record of Neoarchaean to Palaeoproterozoic environmental history. Earth Sci. Rev. 172, 140–177. https://doi.org/10.1016/j.earscirev.2017.06.012.

Large, R.R., Hazen, R.M., Morrison, S.M., Gregory, D.D., Steadman, J.A., Mukherjee, I., 2022. Evidence that the GOE was a prolonged event with a peak around 1900 Ma. Geosyst. Geoenviron. 1 (2), 100036. https://doi.org/10.1016/j.geogeo.2022.100036.

Liu, Z., Algeo, T.J., Brocks, J.J., van Maldegem, L.M., Gilleaudeau, G.J., Kah, L.C., Yu, W., 2025. Salinity reconstruction in Proterozoic depositional systems. Geol. Soc. Am. Bull. 137 (1–2), 447–464. https://doi.org/10.1130/B37489.1.

Lobato, L.M., Ribeiro-Rodrigues, L.C., Vieira, F.W., 2001. Brazil's premier gold province. Part II: geology and genesis of gold deposits in the Archean Rio das Velhas greenstone belt, Quadrilátero Ferrífero. Mineral. Deposita 36, 249–277. https://doi.org/10.1007/s001260100180.

Lyons, T.W., Severmann, S., 2006. A critical look at iron paleoredox proxies: New insights from modern euxinic marine basins. Geochim. Cosmochim. Acta 70 (23), 5698–5722. https://doi.org/10.1016/j.gca.2006.08.021.

Machado, N., Schrank, A., Noce, C.M., Gauthier, G., 1996. Ages of detrital zircon from Archean-Paleoproterozoic sequences: implications for Greenstone Belt setting evolution of a Transamazonian foreland basin in Quadrilátero Ferrífero, Southeast Brazil. Earth Planet. Sci. Lett. 141, 259–276. https://doi.org/10.1016/0012-821X(96)00054-4.

Madeira, M.R., de Souza Martins, M., Martins, G.P., Alkmim, F.F., 2019. Caracterização faciológica e evolução sedimentar da Formação Moeda (Supergrupo Minas) na porção noroeste do Quadrilátero Ferrífero, Minas Gerais. Geol. USP. Série Cient. 19 (3), 129–148. https://doi.org/10.11606/issn.2316-9095.v19-148467.

Madureira, R.D.S., Martins, M., Queiroga, G., Lana, C., Dutra, L.F., Alkmim, A.R., 2021. Depositional setting and U-Pb detrital record of rift-related deposits in the Moeda Formation (Minas Supergroup) at the Gandarela and Ouro Fino synclines, Quadrilátero Ferrífero, Brazil. Brazili. J. Geol. 51 (03), e20200023. https://doi.org/10.1590/2317-4889202120200023.

Marshak, S., Alkmim, F.F., 1989. Proterozoic contraction/extension tectonics of the southern São Francisco region, Minas Gerais, Brazil. Tectonics 8 (3), 555–571. https://doi.org/10.1029/TC008i003p00555.

März, C., Poulton, S.W., Beckmann, B., Küster, K., Wagner, T., Kasten, S., 2008. Redox sensitivity of P cycling during marine black shale formation: dynamics of sulfidic and anoxic, non-sulfidic bottom waters. Geochim. Cosmochim. Acta 72 (15), 3703–3717. https://doi.org/10.1016/j.gca.2008.04.025.

Mendes, M.D.C.O., Lobato, L.M., Suckau, V., Lana, C., 2014. Datação U-Pb in situ por LA-ICPMS em zircões detríticos da Formação Cercadinho, Supergrupo Minas. Geol. USP. Série Científica 14 (1), 55–68. https://doi.org/10.5327/Z1519-874X201400010004.

Mendes, M., Lobato, L.M., Kunzmann, M., Halverson, G.P., Rosière, C.A., 2017. Iron isotope and REE+ Y composition of the Cauê banded iron formation and related iron ores of the Quadrilátero Ferrífero, Brazil. Mineral. Deposita 52, 159–180. https://doi.org/10.1007/s00126-016-0649-9.

Millero, F.J., Feistel, R., Wright, D.G., McDougall, T.J., 2008. The composition of Standard Seawater and the definition of the Reference-Composition Salinity Scale. Deep-Sea Res. I 55 (1), 50–72. https://doi.org/10.1016/j.dsr.2007.10.001.

Moreira, J.L.P., Madeira, C.V., Gil, J.A., Machado, M.A.P., 2007. Bacia de Santos. Boletim Geoci. Petrobr. 15 (2), 531–549.

Morgan, R., Orberger, B., Rosière, C.A., Wirth, R., da Mota Carvalho, C., Bellver-Baca, M. T., 2013. The origin of coexisting carbonates in banded iron formations: a micro-mineralogical study of the 2.4 Ga Itabira Group, Brazil. Precambrian Res. 224, 491–511. https://doi.org/10.1016/j.precamres.2012.10.013.

Nunes, F.S., 2016. Contribuição à estratigrafia e geocronologia U-Pb de zircões detríticos da Formação Moeda (Grupo Caraça, Supergrupo Minas) na Serra do Caraça, Quadrilátero Ferrífero, Minas Gerais. Dissertation on Graduate Program in Geology. Escola de Minas, Universidade de Ouro Preto, Ouro Preto, p. 77.

Oliveira, E.P., Windley, B.F., Araújo, M.N.C., 2010. The Neoproterozoic Sergipano orogenic belt, NE Brazil: a complete plate tectonic cycle in western Gondwana. Precambrian Res. 181 (1), 64–84. https://doi.org/10.1016/j.precamres.2010.05.014.

Olson, H.C., Scheirer, A.H., Ritzer, S.R., Sperling, E.A., 2025. Prediction of organic geochemical parameters from inorganic geochemical data in the Cretaceous-Danian Moreno Formation, San Joaquin Basin, California. Chem. Geol. 674, 122551. https://doi.org/10.1016/j.chemgeo.2024.122551.

Pasquier, V., Fike, D.A., Révillon, S., Halevy, I., 2022. A global reassessment of the controls on iron speciation in modern sediments and sedimentary rocks: a dominant role for diagenesis. Geochim. Cosmochim. Acta 335, 211–230. https://doi.org/10.1016/j.gca.2022.08.037.

Playter, T., Konhauser, K., Owttrim, G., Hodgson, C., Warchola, T., Mloszewska, A.M., Gingras, M., 2017. Microbe-clay interactions as a mechanism for the preservation of organic matter and trace metal biosignatures in black shales. Chem. Geol. 459, 75–90. https://doi.org/10.1016/j.chemgeo.2017.04.007.

Potter, P.E., Shimp, N.F., Witters, J., 1963. Trace elements in marine and fresh-water argillaceous sediments. Geochim. Cosmochim. Acta 27 (6), 669–694. https://doi.org/10.1016/0016-7037(63)90019-X.

Poulton, S.W., Canfield, D.E., 2005. Development of a sequential extraction procedure for iron: implications for iron partitioning in continentally derived particulates. Chem. Geol. 214 (3–4), 209–221. https://doi.org/10.1016/j.chemgeo.2004.09.003.

Poulton, S.W., Canfield, D.E., 2011. Ferruginous conditions: a dominant feature of the ocean through Earth's history. Elements 7 (2), 107–112. https://doi.org/10.2113/gselements.7.2.107.

Raiswell, R., Hardisty, D.S., Lyons, T.W., Canfield, D.E., Owens, J.D., Planavsky, N.J., Reinhard, C.T., 2018. The iron paleoredox proxies: a guide to the pitfalls, problems and proper practice. Am. J. Sci. 318 (5), 491–526. https://doi.org/10.2475/05.2018.03.

Remírez, M.N., Algeo, T.J., Shen, J., Liu, J., Gilleaudeau, G.J., Zhou, L., 2024. Low-salinity conditions in the "marine" late Triassic-early Jurassic Neuquén Basin of Argentina: challenges in paleosalinity interpretation. Palaeogeogr. Palaeoclimatol. Palaeoecol. 646, 112216. https://doi.org/10.1016/j.palaeo.2024.112216.

Retallack, G.J., 2020. Boron paleosalinity proxy for deeply buried Paleozoic and Ediacaran fossils. Palaeogeogr. Palaeoclimatol. Palaeoecol. 540. https://doi.org/10.1016/j.palaeo.2019.109536.

Rosière, C.A., Chemale Jr., F., 2000. Brazilian iron formations and their geological setting. Rev. Brasil. Geoci. 30 (2), 274–278.

Rosière, C.A., Rios, F.J., 2004. The origin of hematite in high-grade iron ores based on infrared microscopy and fluid inclusion studies: the example of the Conceição mine, Quadrilátero Ferrífero, Brazil. Economic Geology 99 (3), 611–624.

Rosière, C.A., Spier, C.A., Rios, F.J., Suckau, V.E., 2008. The itabirites of the Quadrilátero Ferrífero and related high-grade iron ore deposits: an overview. Rev. Econ. Geol. 15, 223–254. https://doi.org/10.5382/Rev.15.09.

Rossignol, C., Lana, C., Alkmim, F., 2020. Geodynamic evolution of the Minas Basin, southern São Francisco Craton (Brazil), during the early Paleoproterozoic: climate or tectonic? J. S. Am. Earth Sci. 101, 102628. https://doi.org/10.1016/j.jsames.2020.102628.

Sampaio, G.M.S., Pufahl, P.K., Raye, U., Kyser, K.T., Abreu, A.T., Alkmim, A.R., Nalini Jr., H.A., 2018. Influence of weathering and hydrothermal alteration on the REE and δ^{56}Fe composition of iron formation, Cauê Formation, Iron Quadrangle, Brazil. Chem. Geol. 497, 27–40. https://doi.org/10.1016/j.chemgeo.2018.08.014.

Schier, K., Ernst, D.M., de Sousa, I.M.C., Garbe-Schoenberg, D., Kuhn, T., Hein, J.R., Bau, M., 2021. Gallium-aluminum systematics of marine hydrogenetic ferromanganese crusts: Inter-oceanic differences and fractionation during scavenging. Geochim. Cosmochim. Acta 310, 187–204. https://doi.org/10.1016/j.gca.2021.05.019.

Scott, C., Lyons, T.W., Bekker, A., Shen, Y., Poulton, S.W., Chu, X., Anbar, A.D., 2008. Tracing the stepwise oxygenation of the Proterozoic Ocean. Nature 452, 456–459. https://doi.org/10.1038/nature06811.

Scott, C., Planavsky, N.J., Dupont, C.L., Kendall, B., Gill, B.C., Robbins, L.J., Lyons, T.W., 2013. Bioavailability of zinc in marine systems through time. Nat. Geosci. 6 (2), 125–128. https://doi.org/10.1038/ngeo1679.

Seixas, L.A.R., Bardintzeff, J.M., Stevenson, R., Bonin, B., 2013. Petrology of the high-Mg tonalites and dioritic enclaves of the ca. 2130 Ma Alto Maranhão suite: evidence for a major juvenile crustal addition event during the Rhyacian orogenesis, Mineiro Belt, Southeast Brazil. Precambrian Res. 238, 18–41. https://doi.org/10.1016/j.precamres.2013.09.015.

Simmons, G.C., Maxwell, C.H., 1961. Grupo Tamanduá da Série Rio das Velhas. DNPM 211, 1–31.

Sirocko, F., 1995. Abrupt Change in Monsoonal Climate: Evidence from the Geochemical Composition of Arabian Sea Sediments. Ph. D. dissertation.. University of Kiel.

Slotznick, S.P., Eiler, J.M., Fischer, W.W., 2018. The effects of metamorphism on iron mineralogy and the iron speciation redox proxy. Geochim. Cosmochim. Acta 224, 96–115. https://doi.org/10.1016/j.gca.2017.12.003.

Song, Y., Gilleaudeau, G.J., Algeo, T.J., Over, D.J., Lyons, T.W., Anbar, A.D., Xie, S., 2021. Biomarker evidence of algal-microbial community changes linked to redox and salinity variation, Upper Devonian Chattanooga Shale (Tennessee, USA). GSA Bull. 133 (1–2), 409–424. https://doi.org/10.1130/B35543.1.

Souza, P.C., Müller, G., 1984. Primeiras estruturas algais comprovadas na Formação Gandarela, Quadrilátero Ferrífero.

Sperling, E.A., Melchin, M.J., Fraser, T., Stockey, R.G., Farrell, U.C., Bhajan, L., Strauss, J.V., 2021. A long-term record of early to mid-Paleozoic marine redox change. Sci. Adv. 7 (28), eabf4382. https://doi.org/10.1126/sciadv.abf4382.

Spier, C.A., Oliveira, S.M., Sial, A.N., Rios, F.J., 2007. Geochemistry and genesis of the banded iron formations of the Cauê Formation, Quadrilátero Ferrífero, Minas Gerais, Brazil. Precambrian Res. 152, 170–206. https://doi.org/10.1016/j.precamres.2006.10.003.

Środoń, J., 2010. Evolution of boron and nitrogen content during illitization of bentonites. Clay Clay Miner. 58, 743–756. https://doi.org/10.1346/CCMN.2010.0580602.

Stookey, L.L., 1970. Ferrozine - a new spectrophotometric reagent for iron. Anal. Chem. 42 (7), 779–781.

Strugale, M., Cartwright, J., 2022. Tectono-stratigraphic evolution of the rift and post-rift systems in the Northern Campos Basin, offshore Brazil. Basin Res. 34 (5), 1655–1687. https://doi.org/10.1111/bre.12674.

Taylor, S.R., McLennan, S.M., 1985. The Continental Crust: Its Composition and Evolution. Blackwell, Oxford, p. 312. https://doi.org/10.1017/S0016756800032167.

Teixeira, N.L., Caxito, F.A., Rosière, C.A., Pecoits, E., Vieira, L., Frei, R., Poitrasson, F., 2017. Trace elements and isotope geochemistry (C, O, Fe, Cr) of the Cauê iron formation, Quadrilátero Ferrífero, Brazil: evidence for widespread microbial dissimilatory iron reduction at the Archean/Paleoproterozoic transition. Precambrian Res. 298, 39–55. https://doi.org/10.1016/j.precamres.2017.05.009.

Tostevin, R., Mills, B.J., 2020. Reconciling proxy records and models of Earth's oxygenation during the Neoproterozoic and Palaeozoic. Interface Focus 10 (4), 20190137. https://doi.org/10.1098/rsfs.2019.0137.

Tribovillard, N., Algeo, T.J., Lyons, T., Riboulleau, A., 2006. Trace metals as paleoredox and paleoproductivity proxies: an update. Chem. Geol. 232 (1–2), 12–32. https://doi.org/10.1016/j.chemgeo.2006.02.012.

Vale, S.A., 2024. Report 20-F. U.S. Securities and Exchange Commission on April 18, 2024, p. 240. https://ri-vale.mz-sites.com/informacoes-para-o-mercado/relatorios-anuais/relatorio-20-f/. accessed 5 February 2025.

Wang, H.Y., Liu, A., Li, C., Feng, Q., Tang, S., Cheng, M., Algeo, T.J., 2021. A benthic oxygen oasis in the early Neoproterozoic Ocean. Precambrian Res. 355. https://doi.org/10.1016/j.precamres.2020.106085.

Wei, W., Algeo, T.J., 2020. Elemental proxies for paleosalinity analysis of ancient shales and mudrocks. Geochim. Cosmochim. Acta 287, 341–366. https://doi.org/10.1016/j.gca.2019.06.034.

Wei, W., Algeo, T.J., Lu, Y., Lu, Y., Liu, H., Zhang, S., Chen, L., 2018. Identifying marine incursions into the Paleogene Bohai Bay Basin lake system in northeastern China. Int. J. Coal Geol. 200, 1–17. https://doi.org/10.1016/j.coal.2018.10.001.

Wei, W., Yu, W., Du, Y., Algeo, T.J., Li, Z., Cheng, M., Konhauser, K., 2024. A new salinity-based model for Cryogenian Mn-carbonate deposits. Precambrian Res. 403, 107309. https://doi.org/10.1016/j.precamres.2024.107309.

Winter, W.R., Jahnert, R.J., França, A.B., 2007. Bacia de Campos. Boletim Geoci. Petrobr. 15 (2), 511–529.

Xu, J., Liu, Z., Bechtel, A., Meng, Q., Sun, P., Jia, J., Song, Y., 2015. Basin evolution and oil shale deposition during Upper cretaceous in the Songliao Basin (NE China): implications from sequence stratigraphy and geochemistry. Int. J. Coal Geol. 149, 9–23. https://doi.org/10.1016/j.coal.2015.07.005.

Yu, W., Algeo, T.J., Zhou, Q., Wei, W., Yang, M., Li, F., Du, Y., Pan, W., Wang, P., 2022. Evaluation of alkalinity sources to Cryogenian cap carbonates, and implications for cap carbonate formation models. Glob. Planet. Chang. 217. https://doi.org/10.1016/j.gloplacha.2022.103949.

Zhang, X., Lin, C., Zahid, M.A., Jia, X., Zhang, T., 2017. Paleosalinity and water body type of Eocene Pinghu Formation, Xihu depression, East China Sea Basin. J. Pet. Sci. Eng. 158, 469–478. https://doi.org/10.1016/j.petrol.2017.08.074.